

Paleoelevations in the Jianchuan Basin of the southeastern Tibetan Plateau based on stable isotope and pollen grain analyses

Jing Wu^{a,b}, Kexin Zhang^{a,b,*}, Yadong Xu^a, Guocan Wang^a, Carmala N. Garzione^{c,*}, John Eiler^d, Philippe Hervé Leloup^e, Philippe Sorrel^e, Gweltaz Mahéo^e

^a School of Earth Sciences, China University of Geosciences, Wuhan 430074, China

^b State Key Laboratory of Biogeology and Environmental Geology, China University of Geosciences, Wuhan 430074, China

^c Department of Earth and Environmental Sciences, University of Rochester, 227 Hutchison Hall, Rochester, NY 14627, USA

^d Division of Geological and Planetary Sciences, California Institute of Technology, Pasadena, CA 91125, USA

^e Université Lyon 1, ENS de Lyon, UMR 5276 CNRS, LGL-TPE, F-69622, Villeurbanne, France

ARTICLE INFO

Keywords:

Yunnan
Clumped isotopes
Paleoaltimetry
Palynomorphs

ABSTRACT

The southeastern margin of the Tibetan Plateau (TP) is a key region for understanding the region's surface uplift mechanisms. This study focused on the Jiuziyan and Shuanghe Formations (Fms) in the Jianchuan Basin, both of which include lacustrine calcareous mudstones and marls. Ostracods of the genus *Austrocypris* found within the Jiuziyan and Shuanghe Fms constrain the age of strata to the Late Eocene. This study used two different proxies, i.e. fossil pollen coexistence and the $\delta^{18}\text{O}$ (VPDB) values of carbonate ($\delta^{18}\text{O}_\text{c}$), to reconstruct paleoelevation and the extant paleoenvironment from lacustrine calcareous mudstones and marls preserved in the Eocene stratigraphy of the Jianchuan Basin. The coexistence approach (CA) using pollen data from the Shuanghe Fm indicates a paleoelevation of 1.3–2.6 km above sea level (asl), which would most probably have been associated with a vegetation cover consisting of tropical-subtropical, deciduous, coniferous, broadleaf forests. The reconstructed mean annual air temperature (MAAT) had a value of 16.8–21.7 °C, warmer than today's MAAT (~6 °C). Oxygen isotope results from the Jiuziyan Fm, with/without modification between Eocene and modern Myanmar sea level, suggested that the surface of the Jianchuan Basin was at a paleoelevation between $0.5^{+0.8}_{-0.5}$ km asl and 2.5 ± 0.7 km asl ($\delta^{18}\text{O}_{\text{mw}}$: $-8.9 \pm 1.3\text{‰}$, 2σ). During the Shuanghe Fm sedimentation the paleoelevation was between $0.9^{+0.7}_{-0.7}$ km asl and 2.9 ± 0.6 km asl ($\delta^{18}\text{O}_{\text{mw}}$: $-9.5 \pm 1.1\text{‰}$, 2σ). Our results suggest that a stepwise uplift of Jianchuan Basin and crustal thickening initiated during the Eocene was the cause of passive surface uplift of the southeastern Tibetan Plateau (TP) rather than Miocene lower crustal flow.

1. Introduction

The Tibetan Plateau (TP) is a result of the tectonic convergence of the Indian and Eurasian continental plates since their initial collision at ~65–50 Ma (Molnar and Tapponnier, 1975; Decelles et al., 2002; Zhang et al., 2008). The southeastern TP is widely considered to be the result of the amalgamation of the Qiangtang and Songpan-Garze blocks to the north with the Indochina and South China blocks to the south (Fig. 1), and as such reflects the dynamic interaction between processes at the Earth's surface and within its lower crust. The southeastern TP, as well as the eastern and central TP, and including the Qiangtang Terrane, all experienced an ultrapotassic magmatic episode around the Eocene-Oligocene boundary (Chung et al., 1998; Wang et al., 2001; Chung et al., 2005; Liang et al., 2007; Lu et al., 2012). When the left-lateral strike-slip along the Ailao Mountains-Red River Fault Zone began

remains debated, with suggestions ranging from 36 Ma to 30 Ma (Zhang and Schärer, 1999; Gilley et al., 2003; Leloup et al., 2007; Cao et al., 2011; Palin et al., 2013). Previous research on low-temperature thermochronometry and geomorphology has suggested that major incision, inferred to reflect surface uplift of the eastern margin of Tibet and the western margin of Sichuan began in the Middle to Late Miocene (Kirby et al., 2002; Clark et al., 2004, 2005; Enkelmann et al., 2006; Godard et al., 2009; Ouimet et al., 2010; Wilson and Fowler, 2011), although more recent thermochronometry data have identified an Oligocene phase of growth in this region (Wang et al., 2012).

The depositional and basin evolution of the Jianchuan area in the southeastern Tibetan Plateau have been the subject of much recent debate (Xiang et al., 2009; Ma, 2013; Zhang et al., 2013; Hoke et al., 2014; Wei et al., 2016; Gourbet et al., 2017; Sorrel et al., 2017). The BGMRY (1990) suggested that the Shuanghe and Jianchuan Fms were

* Corresponding authors.

E-mail addresses: kx_zhang@cug.edu.cn (K. Zhang), carmala.garzione@rochester.edu (C.N. Garzione).

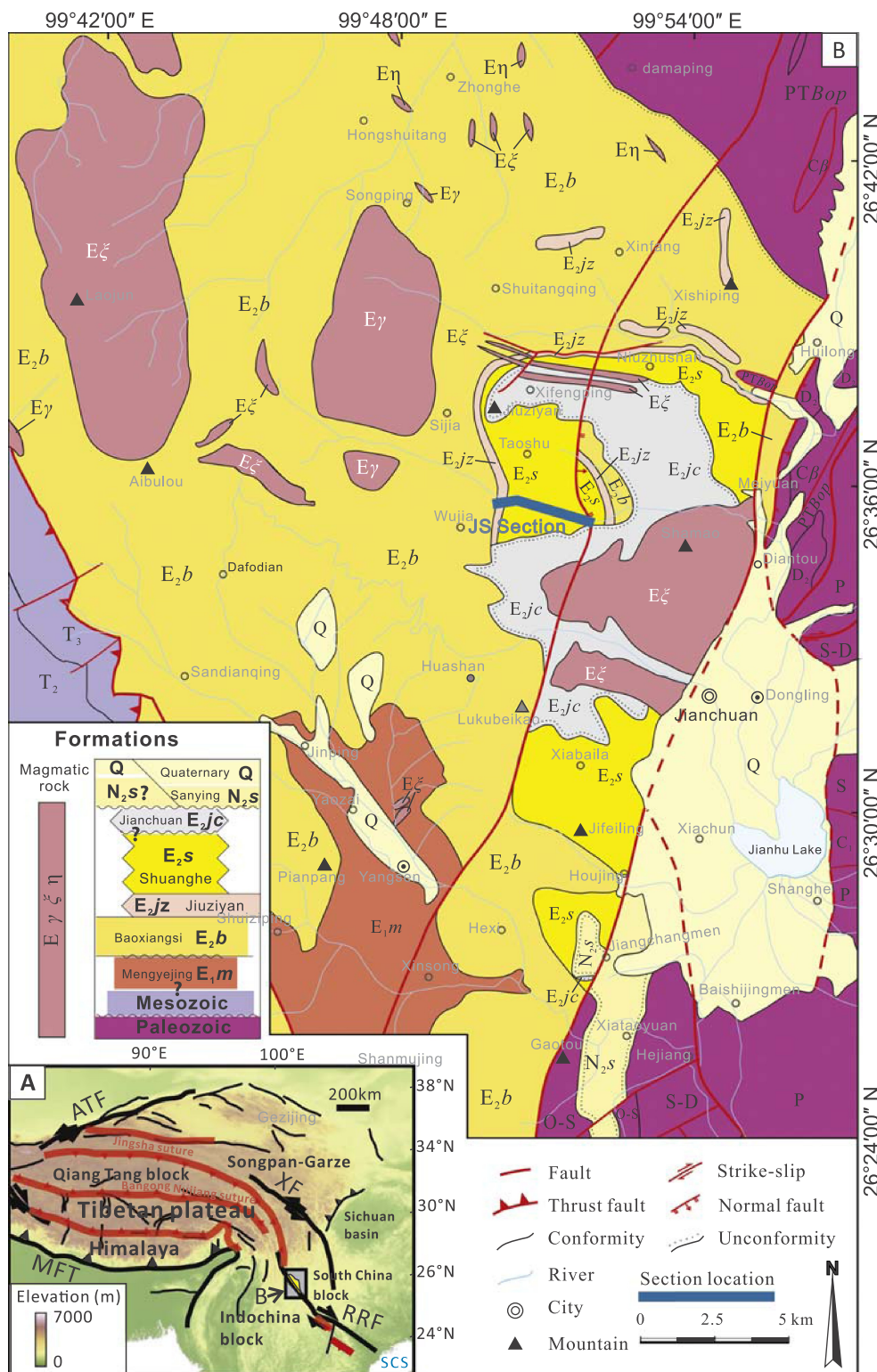


Fig. 1. A. Topographic map of the Tibetan Plateau (colors as a function of elevation from a 1-km-resolution SRTM dataset) with main active faults (black) and suture zones (red). Location of this study (Jianchuan Basin) in the southeastern of Tibetan Plateau in northwest Yunnan Province is shown with the frame corresponds to B. B. Geologic map of the Jianchuan Basin based on existing maps revisited after fieldwork showing Jiuziyan Fm with Shuanghe Fm and the location of the JS Section. The inset in the middle left side depicts the geometrical sedimentary relationships between the formations, with blanks corresponding to sedimentation gaps and undulations to angular unconformities. Magmatic rocks lithology: ξ syenite, γ granite, η norite. (For interpretation of the references to colour in this figure legend, the reader is referred to the web version of this article.)

deposited during the Middle Miocene. In addition, Xiang et al. (2009) proposed that the Shuanghe Fm had a depositional age of 15 Ma, based on geological analysis combined with FT-chronology. However recent LA-ICPMS U-Pb zircon and biotite Ar/Ar ages imply that the Jianchuan Formation is $\sim 35.9 \pm 0.9$ Myr old (Gourbet et al., 2017), confirming earlier U/Pb zircon ages on tuffs of the Jianchuan Fm at 36.34 ± 0.27 Ma (Ma, 2013) and 37.1 ± 1.59 Ma (Hoke et al., 2014).

Existing paleoelevation constraints are only deduced from the $\delta^{18}\text{O}$

values of pedogenic carbonates (Hoke et al., 2014), or marls and shell material (Li et al., 2015). Hoke et al. (2014) suggested that the south-eastern margin of the TP in the Liming Basin has been at an elevation of 2650 ± 300 masl since the Eocene, and that the Jianchuan Basin has been at an elevation of 3300 ± 500 masl since the Middle Miocene. This latter assertion was based upon the dating of volcanoclastic sandstone at the base of the Jianchuan Basin section to ~ 37.1 Ma that bracketed the maximum age of deposition and citing Middle Miocene

age constraints for Jianchuan Basin deposits from other sources (BGMRY, 1990). Hoke et al. (2014) thus suggested that paleoelevations and the geographical extent of the TP during the Eocene were similar than today. Li et al. (2015) used marls and shell from the Shuanghe Fm to suggest that the Jianchuan Basin attained a paleoelevation of 2601 (+802/−1140) m asl during the period ~26–13 Ma. However, the age of the Shuanghe Fm is now demonstrated to be Eocene, not Miocene, which jeopardizes these results. According to the same authors, the nearby Markam Basin had a paleoelevation of 3987 (+1108/−1574) m asl over the same time period. These authors thus speculated that crustal thickening associated with the initiation of the Indian-Eurasian continental collision, or alternatively lower crustal flow in the Lhasa and Qiangtang blocks during the Paleocene-Eocene, was the main reason for the existence of near-modern elevations in northwestern Yunnan since ~40 Ma.

To determine the paleoelevation and paleoenvironmental history of the southeastern TP, we chose an Upper Eocene section in the Jianchuan Basin. The Upper Eocene strata belong to the Baoxiangsi, Jiuziyan, Shuanghe and Jianchuan Fms. This study is focused on the Jiuziyan and Shuanghe Fms. To reduce the potential uncertainties in paleoelevation reconstruction associated with one single proxy, we use two different and complementary proxies, i.e., pollen assemblages and $\delta^{18}\text{O}$ values from calcareous mudstones and marls, in order to reconstruct the Late Eocene elevation history of the southeastern TP. We further incorporate the results from the Coexistence Approach (CA) to account for the additional changes in climate associated with plateau uplift, in order to provide a more conservative estimate of the magnitude of southeastern TP surface uplift during the Late Eocene.

2. Geological background and stratigraphy of the Jianchuan Basin

Our study area, the Jianchuan Basin, is the largest Cenozoic basin of the southeastern Tibetan Plateau and Yunnan Province (Fig. 1). The Basin is rhomb-shaped, with an area of ~2185 km². It extends south-north over a distance of ~130 km, with a width of 30–33 km. The present elevations of this Basin vary from ~2000 m to 4500 m asl. It is bounded by the Qiaohou thrust belt to the west and by the Jianchuan Fault to the east.

The Cenozoic sedimentary rocks reside at modern elevations between 2300 m and 3500 m asl and consist mainly of seven formations. From the bottom to the top of the stratigraphy, these are the Mengyejing, Baoxiangsi, Jinsichang, Jiuziyan and Shuanghe Fms, as well as the Jianchuan Fm, which erupted unconformably over the Shuanghe Fm. The uppermost formation is the Sanying Fm.

The Jiuziyan-Shuanghe (JS) Section (99°50′09″ E, 26°35′38″ N; 2531 m asl) used in this study is located in the east-central part of the Jianchuan Basin, near the Shuanghe coal mine. The Jiuziyan and Shuanghe Fms are exposed here (Figs. 1, 2B).

The Jiuziyan Fm is conformable over the Baoxiangsi Fm in this area and has a thickness of ~20–60 m. The Jiuziyan Fm is mainly characterized by limestone deposits, which have been interpreted as mostly representing a marine environment, according to previous fossil studies (Li et al., 1987). However, a recent study based on new fieldwork and microfacies data clearly demonstrate that it is a palustrine-lacustrine environment (Sorrel et al., 2017). The Jiuziyan Fm has been assigned a Paleocene to Middle Eocene age based on the fossil assemblages by Li et al. (1987). In the JS Section, the Jiuziyan Fm has a thickness of 36 m (Fig. 2A). It is characterized mainly by micritic and micropar to spar limestones, with interbedded marls and conglomerates. The base of the Jiuziyan Fm is characterized by purple and light grey claystone with grey interbedded marls (Fig. 2B). The upper part of the section is characterized by grey micritic limestones and sparitic limestone (Fig. 2B), including fossil reeds and stromatolites, as well as granule to pebbly conglomerates (Sorrel et al., 2017).

The Shuanghe Fm has a thickness of up to ~400 m and consists mainly of mudstones and coal beds interbedded with sandstones. The

Shuanghe Fm was initially described as being Miocene in age based on the presence of a variety of fossils, including plants, bivalves and gastropods (BGMRY, 1996). However, radiometric dating of inter-stratified volcanosedimentary rocks and cross-cutting magmatic rocks demonstrate that the sedimentation of the Shuanghe Fm took place in a short time interval at $\sim 35.9 \pm 0.9$ Ma (Gourbet et al., 2017). In the study section, the Shuanghe Fm is ~157 m thick and is characterized by yellow calcareous mudstones, sandstones with minor conglomerates and coal beds (Fig. 2A). Significant coal deposits occur in layers 66–67, interbedded within yellow sandstones and dark grey calcareous mudstones (Fig. 2B). These deposits include fossil plants, bivalves, gastropods and ostracods. The deposition of the Shuanghe Fm principally took place in a palustrine-lacustrine environment with swamp-like alluvial-palustrine subfacies (Sorrel et al., 2017). While the Shuanghe Fm is conformable on top of the underlying Jiuziyan Fm, the volcanic rocks of the Jianchuan Fm erupted unconformably over the Shuanghe Fm (Gourbet et al., 2017). According to these authors the sedimentation was fast and sedimentation rates rather high in the Jianchuan Basin as the Shuanghe Fm was dated to $\sim 35.9 \pm 0.9$ Ma and the Jianchuan Fm to $\sim 35.4 \pm 0.8$ Ma (Gourbet et al., 2017). Because of uncertainties in age it is impossible to calculate precise sedimentation rates. However, the Shuanghe Fm is ~200 m thick and deposited in < 1.8 Myr which would correspond to a maximum sedimentation rate of ~0.1 mm/yr. The Jianchuan Fm is mostly made of volcanoclastics and may thus have been deposited in a short time interval of a few hundred to a few thousands of years.

3. Methods and material analysis

3.1. Ostracod fossils

We collected 64 bulk samples from limestones within the Jiuziyan Fm, and 150 bulk samples from marls and mudstones within the Shuanghe Fm. About 80–90 g marl and mudstone samples were pre-treated with 15–17% H₂O₂; the heating-acid-digestion method was then applied to marls and mudstones using pure acetic acid. We selected well-preserved specimens for scanning electronic microscope (SEM) photography. Samples were processed at the State Key Laboratory of Biological and Environmental Geology (China University of Geosciences).

3.2. Pollen fossils

A total of 130 bulk samples were collected from mudstone and siltstone deposits within the Shuanghe Fm for pollen grain analysis. About 50–60 g sedimentary samples were treated with 18% HCl and 39% HF to remove carbonates and silica, respectively. Samples were sieved using a 10 μm sieve before the application of ZnCl₂ (density = 2.1) to separate any palynomorphs from the residue, following the method of Faegri and Iversen (1989). Finally, the palynomorphs were mounted in glycerin jelly. All the samples were studied under a light microscope at 400 \times magnification at the State Key Laboratory of Biological and Environmental Geology (China University of Geosciences). Pollen identification followed the methods propounded by Song et al. (1999) and Zhu et al. (1985).

3.3. The coexistence approach (CA)

The CA has been used for Tertiary quantitative terrestrial paleoclimatic reconstructions (Wolfe, 1993; Mosbrugger and Utescher, 1997), including the estimation of paleoelevation (e.g., Utescher et al., 2009; Sun et al., 2014; Miao et al., 2016). This method aims to reconstruct the ranges in paleoelevation and paleotemperature from the nearest living relatives (NLRs) of fossil pollen taxa. The maximum overlap of the environmental tolerances of all the nearest living relatives is regarded as being indicative of the most likely paleoenvironment (Mosbrugger

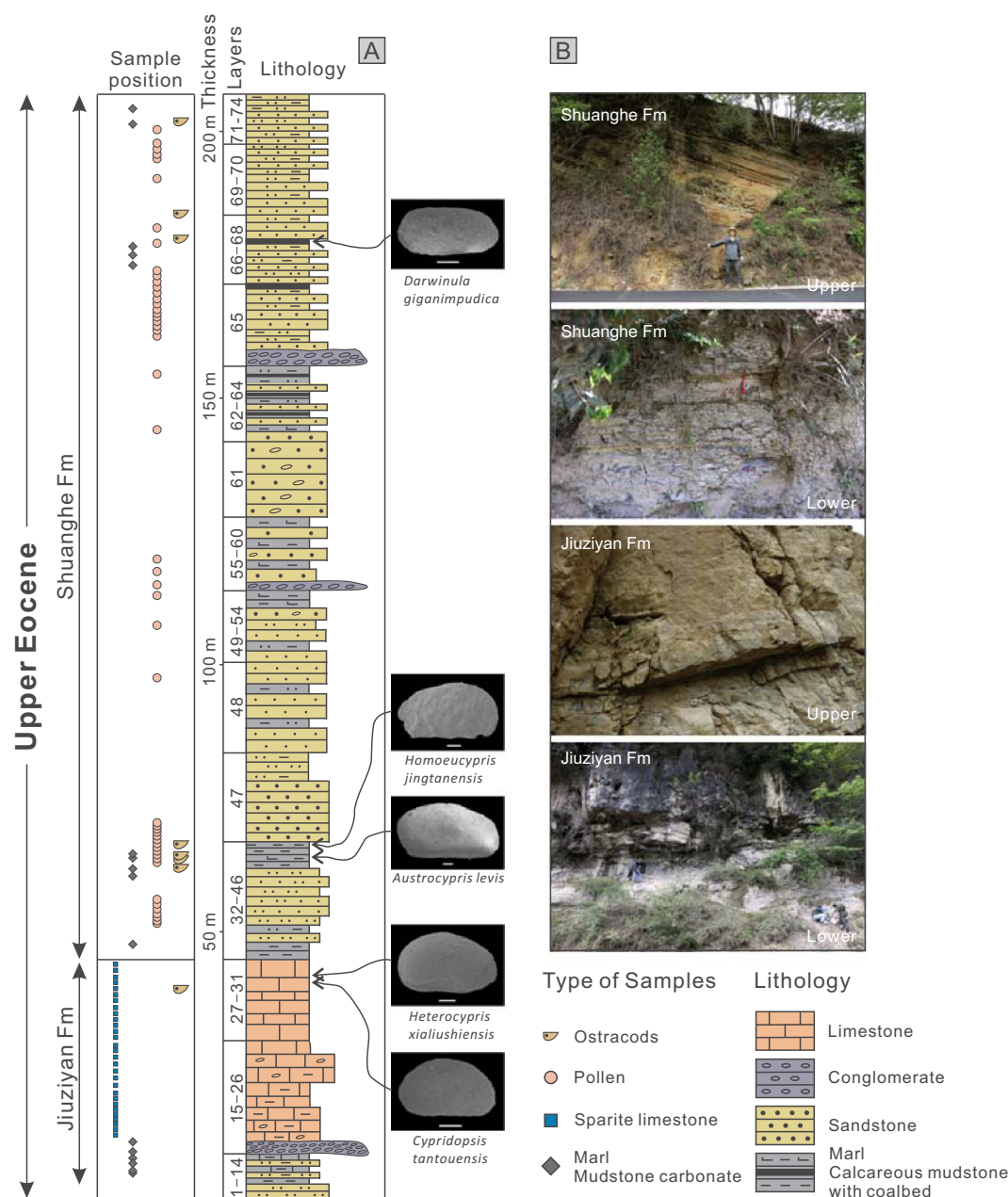


Fig. 2. A. Generalized lithologic column of Jiuziyan and Shuanghe Formations. Inferred stratigraphic position of the sampling localities and sample types are shown with respect to the composite lithologic column. Jiuziyan Fm is dominated by lacustrine marls with calcareous mudstone and limestones. Shuanghe Fm is dominated by sandstones and calcareous mudstones with coal and some conglomerate. B. The lower part of Jiuziyan Fm picture shows horizontal beds of calcareous mudstones and marls with limestones. The upper Jiuziyan Fm picture shows thick layer of limestones. The lower Shuanghe Fm picture shows the typical Shuanghe Fm deposits of horizontally laminated calcareous mudstones with sandstones. The upper Shuanghe Fm picture shows interlayered mudstones and sandstones with coal seam.

and Utescher, 1997). NLRs have their own environment on the TP, and these data have been well summarized by previous researchers (e.g., Wu, 1983, 1985, 1986a, 1986b, 1987; Song et al., 2010). The climatic parameters of the NLRs we used were derived from the China Meteorological Data Sharing Service System (<http://data.cma.cn/site/index.html>). We used the published elevation ranges and climatic parameters of modern Tibetan vegetation (NLRs) for comparison with our fossil pollen assemblages. All the climatic parameters of the NLRs were cross-compared with the PALAEOFLOA Database, which was developed by Utescher and Mosbrugger (http://www2.geo.uni-bonn.de/Palaeoflora/Palaeoflora_home.htm).

3.4. Oxygen and carbon isotopes

A total of 29 limestone and 16 marl and calcareous mudstone samples were collected for stable isotope analysis. Samples were inspected using a binocular microscope, and areas with obvious secondary calcite and/or recrystallization were avoided during sub-sampling for stable isotope analysis. Samples were powdered and homogenized using a mortar and pestle. Powders were treated with 30% H_2O_2 for 20 min to remove organic matter. Powders were then allowed to react with phosphoric acid at 70 °C for at least 50 min to produce CO_2 gas, which was analyzed using a Thermo Delta XP continuous flow gas source mass spectrometer in the University of Rochester's SIREAL laboratory. The results are reported using standard delta notation ($\delta^{18}O$ and $\delta^{13}C$) relative to the Vienna PeeDee belemnite

(VPDB) standard ratio. Isotopic ratios are calculated using three in-house standards that were run within analytical sessions and that have been calibrated using international standards, NBS-18, NBS-19, and L-SVEC, which have established values of $\delta^{13}\text{C} = -5.014\text{‰}$ and $\delta^{18}\text{O} = -23.2\text{‰}$, $\delta^{13}\text{C} = +1.95\text{‰}$ and $\delta^{18}\text{O} = -2.20\text{‰}$, and $\delta^{13}\text{C} = -46.6\text{‰}$ and $\delta^{18}\text{O} = -26.7\text{‰}$, respectively. The three in-house standards are Prang, Crayola, and Thermo1 with calibrated isotopic compositions of $\delta^{13}\text{C} = 0.43\text{‰}$ and $\delta^{18}\text{O} = -7.9\text{‰}$, $\delta^{13}\text{C} = +1.44\text{‰}$ and $\delta^{18}\text{O} = -6.4\text{‰}$, and $\delta^{13}\text{C} = -35.7\text{‰}$ and $\delta^{18}\text{O} = -16.8\text{‰}$, respectively. Analytical errors for $\delta^{18}\text{O}$ and $\delta^{13}\text{C}$ are smaller than $\pm 0.12\text{‰}$ (1 σ) for $\delta^{18}\text{O}$ and $\pm 0.06\text{‰}$ (1 σ) for $\delta^{13}\text{C}$.

3.5. Clumped isotopes ($T_{\Delta 47}$)

We chose a subset of carbonate samples (seven marl and calcareous mudstone samples and one ostracod sample) from the Shuanghe Fm and part of the Jiuziyan Fm for clumped isotope analyses ($T_{\Delta 47}$), which were performed on ~ 8 mg aliquots of the carbonate samples at the California Institute of Technology (Caltech) using Thermo MAT 253 mass spectrometers (Eiler and Schauble, 2004; Affek and Eiler, 2006). Samples were analyzed in a common acid bath at 90°C , and gases were purified by running them through a packed GC column held at -20°C (Passey et al., 2010). All measurements were corrected for instrument non-linearity and scale compression using concurrently analyzed reference gases that had been equilibrated at 1000°C or 25°C , following methods described by Dennis et al. (2011). Data corrected in this way are described in the 'Absolute Reference Frame (ARF)'. Carbonate data were additionally corrected for fractionations associated with acid digestion based on observed values for two concurrently analyzed intra-laboratory carbonate standards – TVO4 and CIT Carrara, which were previously established to have average Δ_{47} values of $+0.666\text{‰}$ and $+0.405\text{‰}$ respectively on the absolute reference frame. The average correction applied at this step was $+0.012\text{‰}$.

Clumped isotope thermometry, which uses measurements of the ^{13}C – ^{18}O bond ordering in carbonates to constrain the temperature ($T_{\Delta 47}$) at which the carbonate grew (Ghosh et al., 2006; Eiler, 2007, 2011), can be used to reconstruct the paleotemperatures of surface environments. In carbonates, clumped isotopes characterize the ratio of mass-47 CO_2 ($^{13}\text{C}^{18}\text{O}^{16}\text{O}$) values to mass-44 CO_2 ($^{12}\text{C}^{16}\text{O}^{16}\text{O}$) values, relative to the randomly distributed heavy isotopologue ratio of mass-47/mass-44 (Ghosh et al., 2006). The oxygen isotopic composition in carbonates ($\delta^{18}\text{O}_\text{C}$) depends on the composition of the meteoric water ($\delta^{18}\text{O}_\text{mw}$) and the temperature at which the carbonate precipitated. We use mean $T_{\Delta 47}$ values to constrain the temperature at which the carbonate precipitated and use the corresponding fractionation factors (Kim et al., 2007) to calculate the $\delta^{18}\text{O}_\text{mw}$ values.

4. Results

4.1. Basin age constraints

The ostracod genus *Austrocypris* is an important index fossil. This genus was short-lived in the Late Eocene (Yang et al., 2000; Xiao et al., 2013). It is widely observed in the lower members of the Upper Eocene Xiaganchaigou Fm in the Qaidam Basin (Yang et al., 2000; Ji et al., 2007; Xiao et al., 2013) and has also been found in the fourth member of the Shahejie Fm in the Dongpu Depression (Xu et al., 2004), and in the Bohai Sea Basin in eastern China (Tong and Chen, 1992). The extinction of these ostracods may correspond with the Eocene-Oligocene climate transition that occurred at ~ 34 Ma (Xiao et al., 2013; Song et al., 2013). Additionally, *Heterocypris* can also be used as a chara ostracod index fossil, as it has been widely reported in the Kangtuo Fm (Gaize Basin), in the Shahejiu Fm (Dongpu and Bohai area), in the Dainan Fm (Jiangsu Province), and in the Kongdian Fm (northern China) in the Late Eocene (Jiang et al., 2014).

In this study, a total of 568 ostracods were found and 18 taxa

identified. Through an analysis of ostracod fauna, two ostracod zones were distinguished, including a *Cypridopsis-Heterocypris* zone and an *Austrocypris levis-Homoecypris jingtianensis-Cyprinotus jiangsuensis-Darwinula* zone. The ostracod genus *Austrocypris* was observed in layers 45–46 (Fig. 2) and can therefore be used for regional stratigraphic correlation to bracket the timing of events. The ostracod genus *Heterocypris* was observed in layers 30, 45 and 67 (Fig. 2). These two chara fossil indices, combined with the two ostracod zones, support the inference of a late Eocene age for the Jiuziyan and Shuanghe Fms.

The reported age of the Shuanghe Fm varies greatly according to the authors. Previous assignments of age have been based mainly on plant fossil analyses. Zhao (1965) suggested a Miocene age based on plant fossils found in the Shuanghe coal mine. Xiang et al. (2009) proposed an age of 15 Ma based on fission track dating. Hoke et al. (2014) reported a U–Pb age of $37.1 (+0.8/-1.6)$ Ma at the base of their Jianchuan Basin section, which lies below the Shuanghe Fm. However, no precise location for the sampling was given which prevent its use as a precise stratigraphic constraint. From a systematic study of crosscutting and interbedded magmatic rocks, including 13 new U/Pb ages, Gourbet et al. (2017) concluded that the Shuanghe Fm is 35.9 ± 0.9 Myr old. This is also supported by the documentation of the teeth of a large amynodontid typical of the Upper Eocene Ergilian interval (37.2 to 33.9 Ma) (Gourbet et al., 2017). Recently, Qin (2017) sampled a very fine-grained volcanic lava at the base of the Jianchuan Fm that had erupted unconformably over the Shuanghe Fm. The lava yielded a weighted mean zircon U–Pb LA-ICPMS age of 36.2 ± 0.9 Ma (2 σ). Combining fossil evidence and the absolute ages demonstrates that the Shuanghe Fm was deposited in a short time at ~ 36 Ma.

4.2. Palynological samples and the coexistence approach (CA)

4.2.1. Pollen results

A total of 49 pollen samples met the statistical quantity requirements for a robust assessment of pollen composition. These samples showed a mean pollen count of 138 pollen grains. A total of 31 pollen taxa were identified in these samples, of which broadleaved, coniferous, shrubby, herbaceous and fern taxa occupied 51.9%, 21.6%, 2.9%, 7.8% and 15.8% of the total pollen composition, respectively. Using the constrained incremental sum of squares (CONISS) to trace any major changes in pollen abundance, such pollen compositions suggest that the vegetation observed in the Shuanghe Fm was dominated by tropical-subtropical, deciduous, coniferous broadleaf forests (Fig. 3).

Pollen assemblage analysis showed that deciduous broadleaf taxa are dominated by *Caryapollenites* (10%), *Cupuliferoipollenites* (8.1%), *Alnipollenites* (7.4%), *Juglanspollenites* (7.3%), *Pterocaryapollenites* (5.2%) and *Meliaceoidites* (4.9%). The coniferous taxa are dominated by *Pinuspollenites* (4.2%), *Cedripites* (4.1%), *Podocarpidites* (1.6%), *Keteleeriaepollenites* (2.9%) and *Taxodiaceapollenites* (2.1%). Fern taxa are characterized by *Polypodiaceasporites* (7.7%), *Lygodiumsporites* (5.5%) and *Pterisporites* (2.6%).

4.2.2. The coexistence approach (CA)

Combining our results with the knowledge of the present-day distributions of fossil pollen NLRs, the diversity of the pollen taxa we observed would suggest the existence of a mixed deciduous, coniferous, broadleaf forest before ~ 36 Ma. Taking the pollen taxa as a whole into consideration, we used the CA to estimate a paleoelevation range of between 1300 m and 2600 m asl (Fig. 6). Employing the CA, we deduced the region's mean annual air temperature (MAAT), arriving at a range of between 16.8°C and 21.7°C (Fig. 4). All paleovegetation, paleoelevation and paleoclimate data are listed in Table 1.

4.3. Stable isotope results

4.3.1. $T_{\Delta 47}$ results

Seven marl and lacustrine calcareous mudstone samples were

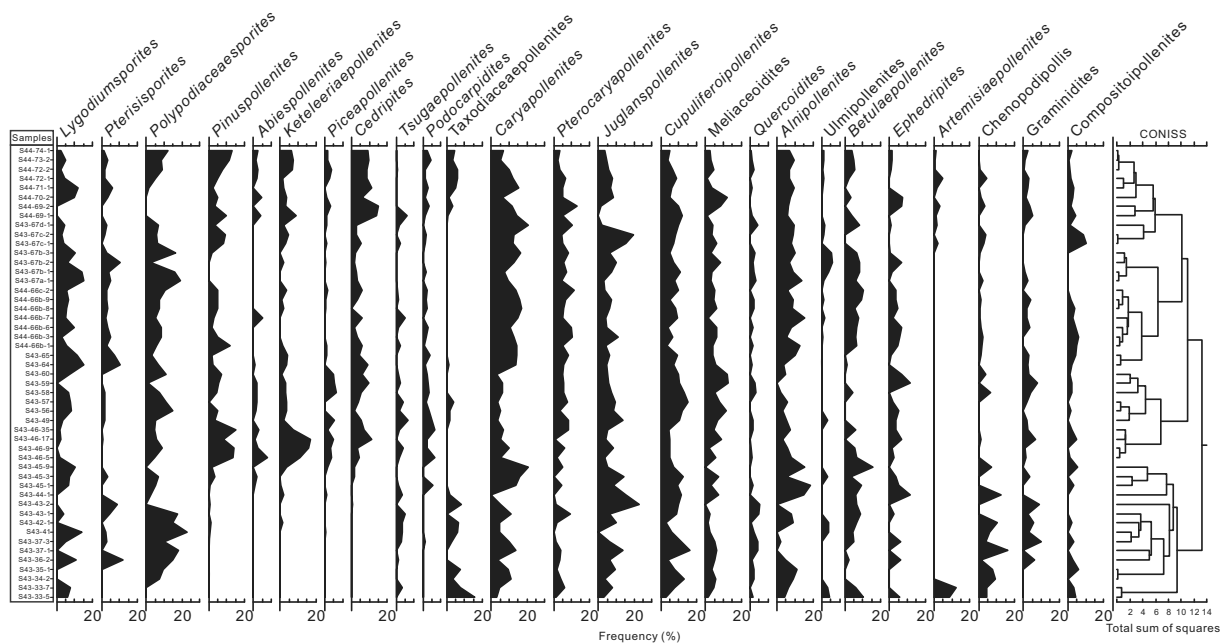


Fig. 3. Pollen diagram showing percentage abundances of pollen taxa within the section, indicating CONISS dendrogram.

chosen for Δ_{47} analysis because these lithologies show micritic textures that have been unaffected by recrystallization. We also collected the shells of the Late Eocene ostracods from an alluvial-lake environment in the Shuanghe Fm (i.e., layers S43-S67d) for clumped isotope

thermometry. All samples were run in duplicate on separate days of analysis. Seven of these eight reproduced with an average standard deviation of $\pm 0.013\text{‰}$, which is comparable to the average standard error of each individual measurement ($\pm 0.014\text{‰}$). But the ostracods

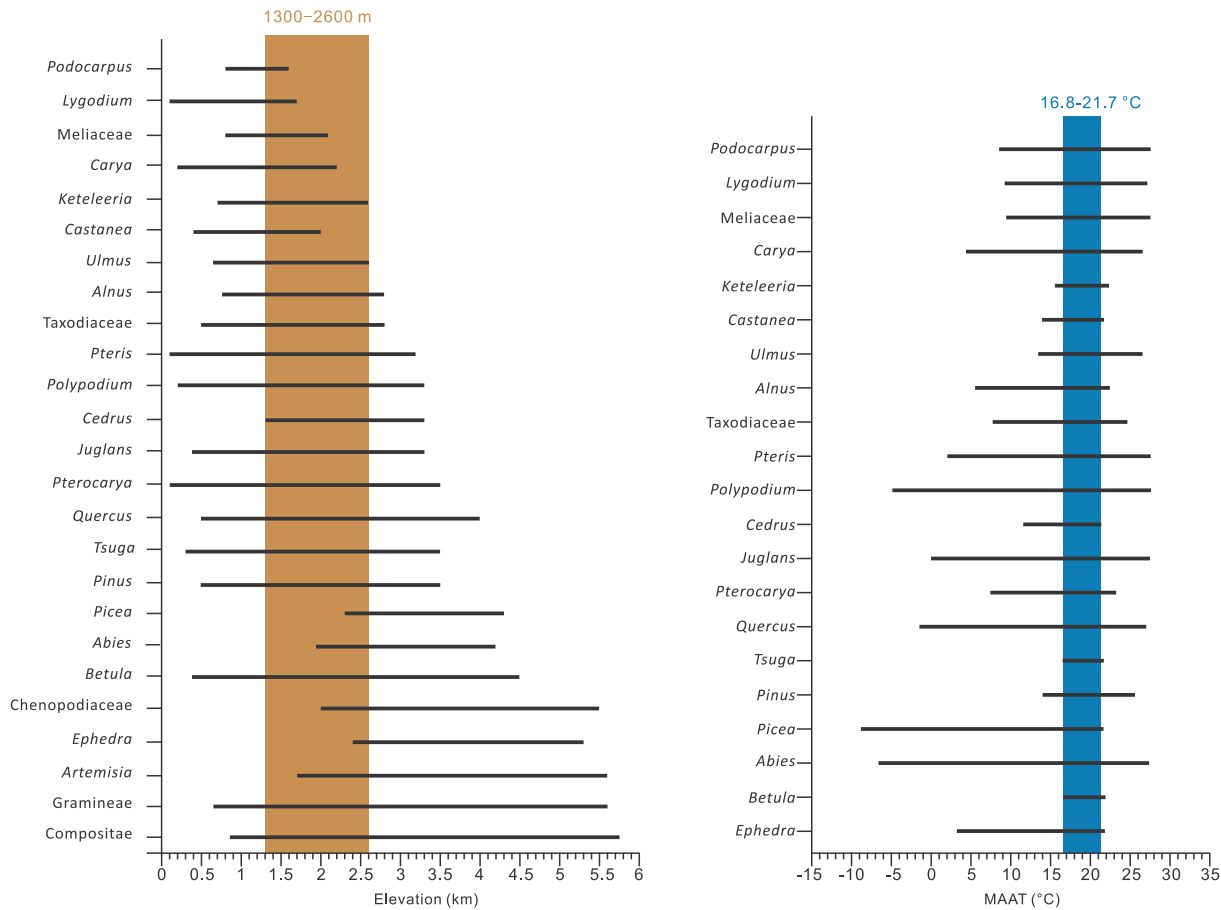


Fig. 4. Plot of altitude ranges and MAAT of presumed nearest living relatives of modern Tibetan vegetation equivalents of fossil pollen taxa recovered from the late Eocene sediments in the Jianchuan Basin.

Table 1Summary of MAAT and modern altitudes of pollen taxa and NLRs^a from the Jianchuan Basin^b.

Pollen taxa	NLRs	MAAT (°C)	Altitude (m)
<i>Lygodiumsporites</i>	<i>Lygodium</i>	9.3–27.1	100–1700
<i>Pterisporites</i>	<i>Pteris</i>	2–27.7	120–3200
<i>Polypodiaceasporites</i>	<i>Polypodium</i>	–4.9–27.7	200–3300
<i>Pinuspollenites</i>	<i>Pinus</i>	14–25.8	500–3500
<i>Keteleeriaepollenites</i>	<i>Keteleeria</i>	15.7–22.2	700–2600
<i>Cedripites</i>	<i>Cedrus</i>	11.6–21.4	1300–3300
<i>Podocarpidites</i>	<i>Podocarpus</i>	8.5–27.7	800–1600
<i>Abiespollenites</i>	<i>Abies</i>	–6.7–27.4	2000–4200
<i>Piceapollis</i>	<i>Picea</i>	–8.9–21.7	2300–4300
<i>Tsugaepollenites</i>	<i>Tsuga</i>	15.7–21.7	300–3500
<i>Taxodiaceapollenites</i>	<i>Taxodiaceae</i>	7.8–24.7	500–2800
<i>Ephedripites</i>	<i>Ephedra</i>	3.1–28.8	2400–5300
<i>Betulaepollenites</i>	<i>Betula</i>	16.8–21.9	400–4500
<i>Juglanspollenites</i>	<i>Juglans</i>	0–27.5	400–3300
<i>Pterocaryapollenites</i>	<i>Pterocarya</i>	7.3–23.1	50–3500
<i>Alnipollenites</i>	<i>Alnus</i>	5.6–22.4	780–2800
<i>Cupuliferoipollenites</i>	<i>Castanea</i>	14–21.8	400–2000
<i>Quercoidites</i>	<i>Quercus</i>	–1.4–27	500–3900
<i>Caryapollenites</i>	<i>Carya</i>	4.4–26.6	200–2200
<i>Meliaceoidites</i>	<i>Meliaceae</i>	9.4–27.7	800–2100
<i>Ulmipollenites</i>	<i>Ulmus</i>	13.3–26.6	650–2600
<i>Artemisiaepollenites</i>	<i>Artemisia</i>	–	1700–5600
<i>Graminidites</i>	<i>Gramineae</i>	–	650–5600
<i>Chenopodiipollis</i>	<i>Chenopodiaceae</i>	–	2000–5500
<i>Compositoipollenites</i>	<i>Compositae</i>	–	850–5750

^a NLRs: nearest living relatives.^b Data of MAAT and modern altitudes of pollen taxa and NLRs from e.g., Wu, 1983, 1985, 1986a, 1986b, 1987; Song et al., 2010.

sample failed to reproduce within expected limits of Δ_{47} and $\delta^{13}\text{C}$ (Table 2). We have no insights into why this sample failed to reproduce, but comparison with other samples in this suite suggests that the anomalously low temperature analysis is the one in error. The TA_{47} values from the Jiuziyan and Shuanghe Fms' carbonate samples of marl and calcareous mudstones showed a large temperature range from 21 °C to 55 °C (Fig. 5 and Table 2).

The TA_{47} values of some of the Eocene Jianchuan Basin samples are well above Earth surface temperatures, and well above the temperature estimates of 16.8 °C to 21.7 °C derived from our pollen analyses (see Section 4.2.2), suggesting some degree of diagenetic resetting. The samples that provided the warmest temperatures were the ostracod shells from the upper part of the Shuanghe Fm, which yielded an apparent temperature of 90 °C (Fig. 5 and Table 3). Of all the carbonates from marls and calcareous mudstones that showed micritic textures, two samples recorded TA_{47} values of > 43 °C. These two samples (i.e., S43-46-5; S43-72-2) were from the Shuanghe Fm and exhibited TA_{47} values of 45–47 °C and 43–55 °C (Fig. 5 and Table 3). The high TA_{47} values and micritic nature of the carbonates would suggest that diagenesis occurred as solid-state C–O bond reordering, which would have altered the Δ_{47} composition without modifying the $\delta^{18}\text{O}$ and $\delta^{13}\text{C}$ compositions (e.g., Huntington et al., 2015). Considering that a significant subset of samples showed evidence for higher temperature C–O bond reordering, we cannot rule out some degree of reordering in all samples, and therefore do not use these values in MAAT and/or paleoelevation reconstructions.

4.3.2. Carbon isotope and oxygen isotope results

The $\delta^{13}\text{C}$ (VPDB) values in the lower strata of the Jiuziyan Fm (i.e., layers S43-4-1 to S43-13-1) show a narrow range from –0.9‰ to –1.5‰, but the strata of the upper Jiuziyan Fm (i.e., layers S43-16-2 to S43-31-25) show a large range in $\delta^{13}\text{C}$ (VPDB) values from –3.7‰ to +7.4‰ (Fig. 6 and Table 1). The Shuanghe Fm shows a moderate variability in $\delta^{13}\text{C}$ (VPDB) values from –4.6‰ to +2.1‰ (Fig. 6).

The $\delta^{18}\text{O}$ (VPDB) values in the lower strata of the Jiuziyan Fm range

between –9.1‰ and –11.9‰, with a mean value of $-10.1 \pm 0.7\text{‰}$ (2 σ) (Fig. 5 and Table 1). In the upper Jiuziyan Fm strata (i.e., S43-16-2 to S43-31-25), $\delta^{18}\text{O}$ (VPDB) values range between –10.3‰ and –18.7‰. The Shuanghe Fm shows small variations in $\delta^{18}\text{O}$ (VPDB) values that range from –10.6‰ to –12.5‰, with a mean value of $-11.6 \pm 0.7\text{‰}$ (2 σ). However, ostracods from layer S43-67 of the Shuanghe Fm recorded a slightly higher $\delta^{18}\text{O}$ (VPDB) value of –9.5‰.

4.4. Diagenetic history

We produced thin sections and analyzed individual carbonate phases for diagenesis. Diagenesis can modify the original isotopic composition of calcareous sediments, potentially resetting the TA_{47} and $\delta^{18}\text{O}$ signatures of carbonates (e.g., Garzzone et al., 2004; Huntington et al., 2015). Diagenetic resetting by mineral recrystallization associated with burial will result in higher TA_{47} values. More negative $\delta^{18}\text{O}_c$ values will also occur if recrystallization takes place in the presence of groundwater. Because recrystallization produces observable coarse crystals or spar, it can be easily distinguished in thin sections. However, solid state reordering of C and O isotopes can alter TA_{47} values without significant change in the micritic texture or $\delta^{18}\text{O}$ and $\delta^{13}\text{C}$ values (Huntington et al., 2015). An examination of thin sections of marl (layer S43-5-1) from the lower Jiuziyan Fm (Fig. 7A), as well as calcareous lacustrine mudstones (layer S43-73-3) from the Shuanghe Fm (Fig. 7B), shows a lack of sparry recrystallization, and few to no veins. In limestone samples from the upper Jiuziyan Fm (i.e., layers S43-26 and S43-30), veins are observed to cross-cut micrite, and some parts of the samples show pervasive recrystallization (Fig. 7C, D). Inspection of samples under a binocular microscope reveals that veins and sparry recrystallization are common diagenetic features throughout the Jiuziyan Fm limestones. To identify the isotopic composition of diagenetic carbonates, we used a dental drill to sub-sample coarse sparite veins in three limestone samples that show pervasive diagenesis. The sparite limestones from the Jiuziyan Fm (upper part) have $\delta^{18}\text{O}_c$ values ranging from –10.3‰ to –15.3‰. The veins in the sparite limestones show $\delta^{18}\text{O}_c$ values ranging from –13.3‰ to –14.7‰; these overlap with the more negative range of the limestone samples (Table 2). Based on observations of the thin sections and the $\delta^{18}\text{O}_c$ values of marls and calcareous mudstones, we infer that limestones from the Jiuziyan Fm record varying degrees of recrystallization, associated with more negative $\delta^{18}\text{O}_c$ values compared with the micritic carbonates from the Jiuziyan Fm.

The regional thickness of the Jiuziyan Fm is ~0.1 km. The younger Formations, including the Shuanghe (~0.2 km), Jianchuan (~0.4 km) and Sanyin (~1.3 km), have a total thickness of ~1.9 km. Therefore, we infer the burial depth of the Jiuziyan Fm to be at least ~2 km. Assuming a mean geothermal gradient of ~25 °C/km and a surface temperature of 20 °C (based on the pollen-derived evidence discussed in Section 5.2.2), these thicknesses most likely indicate that recrystallization took place at a temperature of up to ~70 °C. The $\delta^{18}\text{O}_c$ values of diagenetically altered carbonates also support this inference. For every 4.5 °C increase in temperature (T), there is an approximately –1‰ change in the $\delta^{18}\text{O}_c$ (Kim et al., 2007). Looking at the mean $\delta^{18}\text{O}_c$ values of Jiuziyan micrites ($-10.4 \pm 0.7\text{‰}$), and the most negative sparite limestone (–18.7‰), the difference between them suggests a temperature of diagenesis of ~60 °C, similar to the inferred burial temperature result. These temperatures are lower than the TA_{47} value recorded in the ostracod sample (i.e., 90 °C). However, a (U–Th)/He apatite age suggested that 1.5 to 2.7 km of sediments have been eroded in Oligo-Miocene time from the Jianchuan Basin (Shen et al., 2016). Thus, additional Eocene sediments, in excess of what is preserved today, appear to have been eroded in Oligo-Miocene times. Based on stratigraphic thickness and comparison of the $\delta^{18}\text{O}_c$ values of micrite and diagenetic phases, maximum burial temperatures of 80–90 °C are realistic. Yet another possible explanation for the higher temperature

Table 2 $\delta^{13}\text{C}$ and $\delta^{18}\text{O}$ values of marls, calcareous mudstones and fossil ostracods from the Jianchuan Basin.

Sample No.	Samples height (m)	Formation name	Sample types	$\delta^{13}\text{C}$ (VPDB)	$\delta^{18}\text{O}$ (VPDB)
S43-4-1	4.3	Jiuziyan Fm	Calcareous mudstone	−1.1	−9.4
S43-4-2*	4.4	Jiuziyan Fm	Calcareous mudstone	−0.9	−11.3
S43-5-1	4.7	Jiuziyan Fm	Marl	−1.3	−10.3
S43-9-3*	5.7	Jiuziyan Fm	Marl	−1.4	−10.8
S43-10	5.8	Jiuziyan Fm	Marl	−1.4	−10.0
S43-13-1*	6.2	Jiuziyan Fm	Marl	−1.1	−11.9
S43-16-2*	7.5	Jiuziyan Fm	Sparite limestone	−1.9	−10.3
S43-16-22*	8.5	Jiuziyan Fm	Sparite limestone	−3.7	−11.4
S43-17-1*	9.1	Jiuziyan Fm	Sparite limestone	+1.4	−11.3
S43-18-2*	9.5	Jiuziyan Fm	Sparite limestone	+4.0	−13.2
S43-19-5*	9.9	Jiuziyan Fm	Sparite limestone	+1.1	−12.7
S43-20-4*	10.2	Jiuziyan Fm	Sparite limestone	+3.2	−12.2
S43-21-3*	10.4	Jiuziyan Fm	Sparite limestone	+3.0	−12.6
S43-22-13*	11.2	Jiuziyan Fm	Sparite limestone	+5.7	−11.7
S43-23-6*	11.5	Jiuziyan Fm	Sparite limestone	+4.4	−12.7
S43-24-12*	12.3	Jiuziyan Fm	Sparite limestone	+5.6	−11.4
S43-24-32*	14.2	Jiuziyan Fm	Sparite limestone	+5.8	−11.8
S43-24-54*	16.4	Jiuziyan Fm	Sparite limestone	+0.5	−11.2
S43-25-10*	17.8	Jiuziyan Fm	Sparite limestone	+4.7	−11.5
26-W-11	20.3	Jiuziyan Fm	Sparite	+4.9	−14.7
S43-26-14*	20.4	Jiuziyan Fm	Sparite limestone	+5.5	−11.6
S43-26-34*	22.4	Jiuziyan Fm	Sparite limestone	+5.1	−15.3
S43-26-54*	24.4	Jiuziyan Fm	Sparite limestone	+5.2	−15.4
S43-26-84*	27.3	Jiuziyan Fm	Sparite limestone	+5.4	−14.2
S43-27-4*	28.3	Jiuziyan Fm	Sparite limestone	+6.2	−11.9
S43-27-24*	30.3	Jiuziyan Fm	Sparite limestone	+6.8	−12.6
S43-28-5*	31.2	Jiuziyan Fm	Sparite limestone	+7.1	−11.8
S43-28-15*	32.2	Jiuziyan Fm	Sparite limestone	+5.6	−12.3
S43-28-25*	33.2	Jiuziyan Fm	Sparite limestone	+6.4	−12.5
S43-29-5*	34.2	Jiuziyan Fm	Sparite limestone	+6.1	−11.8
S43-30-1*	35.8	Jiuziyan Fm	Sparite limestone	+6.6	−15.3
30-W-2	35.9	Jiuziyan Fm	Sparite	+7.4	−13.3
S43-30-11*	36.8	Jiuziyan Fm	Sparite limestone	+6.2	−18.7
S43-31-3*	37.7	Jiuziyan Fm	Sparite limestone	+5.7	−14.6
S43-31-25*	39.4	Jiuziyan Fm	Sparite limestone	+0.6	−12.1
S43-33-W-1	44.6	Shuanghe Fm	Calcareous mudstone	−4.4	−12.2
S43-43-6	56.3	Shuanghe Fm	Calcareous mudstone	−1.1	−10.9
S43-44-W-13	57.1	Shuanghe Fm	Marl	+2.0	−10.8
S43-46-W-5	58	Shuanghe Fm	Marl	+0.8	−11.4
S43-46-W-6	58.1	Shuanghe Fm	Marl	+0.7	−12.3
S43-66b-3	167	Shuanghe Fm	Calcareous mudstone	+1.8	−10.9
S43-66b-7	168	Shuanghe Fm	Calcareous mudstone	+0.7	−11.3
S43-67d-1	172.7	Shuanghe Fm	Marl	+0.2	−12.4
S43-72-2	197.9	Shuanghe Fm	Marl	+1.5	−11.9
S43-73-3	201.6	Shuanghe Fm	Calcareous mudstone	+1.4	−10.7

Analyses with precision of $\pm 0.06\text{‰}$ for carbon and $\pm 0.10\text{‰}$ for oxygen; VPDB = Vienna peedee belemnite; the second number in each sample number indicates the different layers of samples within the JS Section (e.g., JS43-4-1 was samples at layer 4); * means the data were collected at Tongji University.

recrystallization of the Jiuziyan Fm limestones is the regional volcanism (Gourbet et al., 2017) during and after the deposition of the Shuanghe Fm. This volcanism may have generated hot fluids that interacted with the limestones.

The stable carbon isotopes of limestones from the Jiuziyan Fm exhibited a wide range in $\delta^{13}\text{C}_\text{c}$ values from -3.7‰ to $+7.4\text{‰}$. This gives further insight into the likely palustrine-lacustrine paleoenvironment (Sorrel et al., 2017). The carbon isotopic composition of limestones is mainly determined by dissolved inorganic carbon (DIC), and DIC in lacustrine water is primarily controlled by the photosynthesis-respiration cycle. In open lakes, primary carbonates record the isotopic composition of DIC in the upper water column at the time of precipitation. The carbon isotopic composition of some of the heavily recrystallized sparite limestone of the Jiuziyan Fm is shifted to more positive $\delta^{13}\text{C}_\text{c}$ values with respect to the micritic carbonates. Bacterial methanogenesis has a strong effect on C isotopic fractionation, with biogenic methane preferentially enriched in ^{12}C , and ^{13}C enriched in the accompanying bicarbonate (Waldron et al., 1999; Jahren et al., 2004; Chanton et al., 2005). The extreme $\delta^{13}\text{C}_\text{c}$ enrichment (up to $+7.4\text{‰}$) observed in limestones from the Jiuziyan Fm is characteristic

of diagenetic carbonates that precipitate in association with bacterial methanogenesis (Talbot and Kelts, 1990). This process sometimes reflects early diagenesis at shallow burial depths, which may explain why some of the sparite limestones that recorded high $\delta^{13}\text{C}_\text{c}$ values did not show a strong deviation to more negative $\delta^{18}\text{O}_\text{c}$ values (e.g., Garzzone et al., 2004).

5. Discussion and interpretation

5.1. New paleotemperature constraints from the late Eocene Jianchuan Basin

Late Eocene Jianchuan flora consists of mesothermic elements such as *Caryapollenites*, *Pterocaryapollenites*, *Cupuliferoipollenites*, *Juglanspollenites*, *Meliaceoidites*, *Alnipollenites*, and *Ulmipollenites*, meso-microthermic elements such as *Taxodiaceapollenites* and *Cryptomeriapollenites*, other conifers as represented by *Pinuspollenites*, *Keteleeriaepollenites*, *Cedripites* and *Podocarpidites*, and herbs such as *Graminidites*, *Compositiipollenites* and *Chenopodipollis*. This flora indicates that vegetation in the Late Eocene was most likely mixed

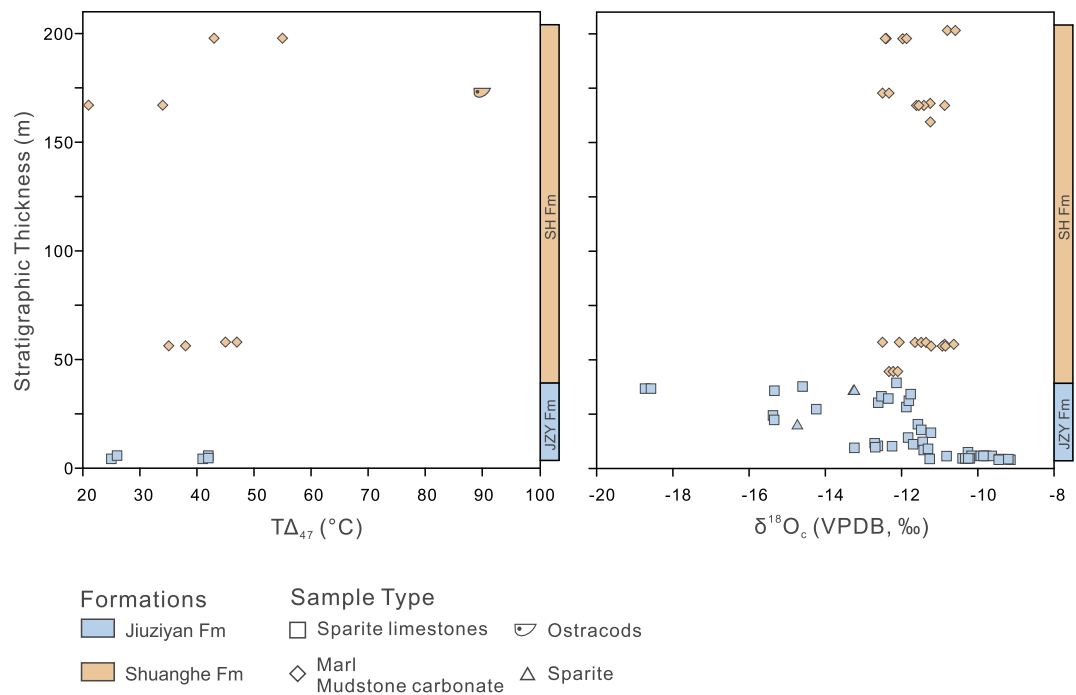


Fig. 5. Isotopic data from carbonate samples plotted against the inferred stratigraphic height. A. Plot of $T\Delta_{47}$ ($^{\circ}\text{C}$) temperatures. B. Plot of $\delta^{18}\text{O}_{\text{mw}}$ (VSMOW) values reconstructed from $\delta^{18}\text{O}_{\text{c}}$ (VPDB).

tropical-subtropical, deciduous, coniferous, broad-leaved forest. In addition, the coexistence of species indicative of sub-tropical, temperate and mountain coniferous forests suggests a vertical zonation of vegetation, and the existence of surrounding higher elevations. Moreover, this palynological assemblage is compatible with that of macroflora described in the Shuanghe Fm of the Jianchuan Basin (Sun et al., 2011).

Based on the climatic preferences of the NLRs, we reconstructed the Late Eocene climate of the Jianchuan Basin, proposing the existence of a warm, subtropical climate, with a MAAT of 16.8–21.7 $^{\circ}\text{C}$, and a mean value of 19.3 ± 2.5 $^{\circ}\text{C}$. These results are compatible with those of Sun et al. (2011): MAAT of 18.2 ± 3.6 $^{\circ}\text{C}$. However, the present climate, which has a MAAT of 13.5 ± 1.4 $^{\circ}\text{C}$ (<http://data.cma.cn/site/index.html>), is much cooler than that of the Eocene.

Climate modeling studies suggest that the Southeast Asian Monsoon was present and robust during the Late Eocene, regardless of the elevation, latitudinal position and width of the Himalayan-Tibetan system

(Huber and Goldner, 2012; Roe et al., 2016). During the summer, the TP would have experienced a significantly warm and moist airflow, which can be associated with the region's climate patterns and the height of the TP (Huber and Goldner, 2012). Recent researchers have evaluated one general circulation model, which appears to be consistent with the strength of the atmospheric circulation and the distribution of precipitation; both these latter parameters are tightly coupled to the spatial patterns of low-level moist static energy and the temperature of the upper troposphere (Roe et al., 2016). Given the similarity between the modern and Eocene monsoonal climate, it would seem reasonable to assume from our pollen-based inferences that the climate was warmer in the Jianchuan Basin during the Eocene than it is now.

Table 3
Summary of clumped isotope data from the Jianchuan Basin.

Sample No.	Samples height (m)	Formation name	Sample types	$\delta^{13}\text{C}$ (PDB) (‰)	$\delta^{13}\text{C}$ stdev	$\delta^{18}\text{O}_{\text{c}}$ (PDB) (‰)	$\delta^{18}\text{O}_{\text{c}}$ stdev	Δ_{47} (Caltech) (‰)	Δ_{47} stdev	Δ_{47} (ARF) (‰)	$T(\Delta_{47})$ (Caltech) ($^{\circ}\text{C}$)
S43-4-1	4.3	Jiuziyan Fm	Calcareous mudstone	−1.1	0.007	−9.2	0.012	−0.2	0.036	0.645	41
S43-4-1	4.3	Jiuziyan Fm	Calcareous mudstone	−1.1	0.006	−9.1	0.015	−0.1	0.058	0.692	25
S43-5-1	4.7	Jiuziyan Fm	Marl	−1.2	0.004	−10.2	0.008	−0.2	0.051	0.644	42
S43-10	5.8	Jiuziyan Fm	Marl	−1.3	0.004	−9.9	0.011	−0.2	0.064	0.644	42
S43-10	5.8	Jiuziyan Fm	Marl	−1.3	0.005	−9.6	0.004	−0.2	0.028	0.689	26
S43-43-6	56.3	Shuanghe Fm	Calcareous mudstone	−1.1	0.005	−11.2	0.015	−0.2	0.062	0.663	35
S43-43-6	56.3	Shuanghe Fm	Calcareous mudstone	−1.1	0.007	−10.9	0.010	−0.2	0.031	0.654	38
S43-46-W-5	58	Shuanghe Fm	Marl	+0.9	0.005	−11.6	0.007	−0.2	0.021	0.634	45
S43-46-W-5	58	Shuanghe Fm	Marl	+0.9	0.006	−11.5	0.021	−0.2	0.033	0.629	47
S44-66b-3	167	Shuanghe Fm	Calcareous mudstone	+1.7	0.003	−11.5	0.018	−0.2	0.050	0.666	34
S44-66b-3	167	Shuanghe Fm	Calcareous mudstone	+1.7	0.007	−11.6	0.007	−0.1	0.022	0.705	21
S44-72-2	197.9	Shuanghe Fm	Marl	+1.5	0.004	−12.4	0.006	−0.2	0.041	0.610	55
S44-72-2	197.9	Shuanghe Fm	Marl	+1.5	0.005	−12.4	0.007	−0.2	0.027	0.641	43
S43-67d	172.7	Shuanghe Fm	Shell	−1.0	0.006	−9.5	0.012	−0.3	0.056	0.537	90

See text for description of absolute reference frame (ARF) and California Institute of Technology (Caltech) reference frames. Fractionation factor for calcite from Kim and O'Neil (1997). Euler use the current calibration (Bonifacie et al., 2017) for Absolute Reference Frame data. VPDB = Vienna PeeDee belemnite; the second number in each sample number indicates the different layers of samples within the JS Section (e.g., JS43-4-1 was sampled at layer 4), SE = Standard Error.

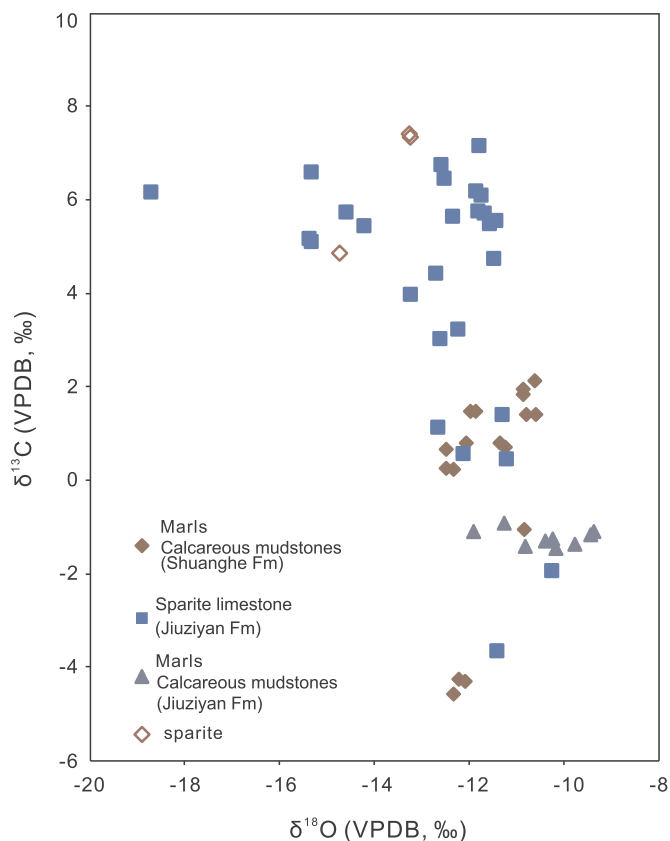


Fig. 6. Correlations between $\delta^{13}\text{C}$ and $\delta^{18}\text{O}$ from primary (micrite) and secondary diagenetic (sparite) carbonates.

5.2. Meteoric water

The degree of covariance between $\delta^{18}\text{O}$ and $\delta^{13}\text{C}$ values in lacustrine carbonates can be used to discriminate between carbonates produced in hydrologically open and hydrologically closed lacustrine environments. Open lakes more closely reflect the bulk isotopic composition of inflow waters, whereas closed lakes may experience a greater degree of evaporative enrichment of ^{18}O , and therefore show more positive $\delta^{18}\text{O}$ values than observed in inflow water. Carbonates that precipitate from open lakes usually show little or no correlation between $\delta^{13}\text{C}$ and $\delta^{18}\text{O}$ values, while closed lake systems precipitate carbonate that often shows a strong covariance between $\delta^{13}\text{C}$ and $\delta^{18}\text{O}$ values (Talbot, 1990). The marls and calcareous mudstones in the Jiuziyuan and Shuanghe Fms lack any significant covariance between $\delta^{13}\text{C}$ and $\delta^{18}\text{O}$ values, exhibiting a relatively narrow range of $\delta^{18}\text{O}$ values from -12.7‰ to -9.7‰ (Fig. 5), suggesting that both lake systems were most likely open (Fig. 6).

The $\delta^{18}\text{O}_c$ values in lacustrine environments may be influenced by multiple factors, such as the $\delta^{18}\text{O}$ value of local meteoric water, evaporation, diagenesis, and the temperature at which calcite precipitates. Mindful of this and based on a lack of covariance between the $\delta^{13}\text{C}$ and $\delta^{18}\text{O}$ values of lacustrine carbonates, and the small range in carbonate $\delta^{18}\text{O}$ values, the micritic texture of the lacustrine marls and calcareous mudstones we analyzed would suggest minimal diagenetic alteration of the $\delta^{18}\text{O}$ values of the primary carbonate. We therefore suggest that $\delta^{18}\text{O}_{\text{mw}}$ is the main determinant of $\delta^{18}\text{O}_c$ in the marl and calcareous mudstone samples of the Late Eocene age from the Jianchuan Basin. Given the evidence for the extensive diagenesis of Jiuziyuan limestones, we do not use limestone samples from the Jiuziyuan Fm in the analysis of paleoelevation.

Paleometeoric water compositions are determined from sedimentary carbonates, assuming reasonable temperatures for carbonate formation. In this study, we used the MAAT derived from our analyses of

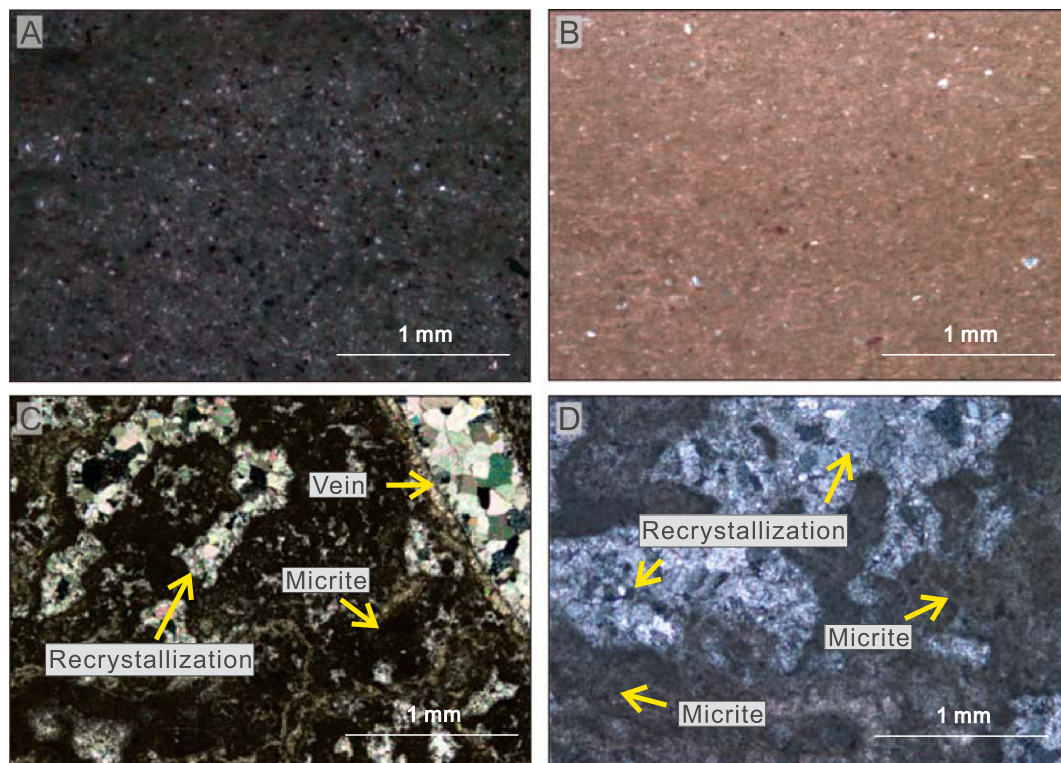


Fig. 7. Photomicrographs of examined thin sections, highlighting the diagenetic features observed in the typical samples and general composition of the same samples. All the pictures were taken under cross-polarized light. A. the Marl from lower part of Jiuziyuan Fm is rich in quartz and clay with 50% carbonate. B. the Shuanghe Fm calcareous mudstone lacks veins and the sparry calcite and consists of 30% carbonate. C. the Jiuziyuan Fm limestone (S43-26-13) shows some recrystallized zones with veins and consists of ~50% unaltered micrite. D. the Jiuziyuan Fm limestone (S43-30-2) shows pervasive recrystallization.

Table 4
Summary of paleoelevation estimates from lower Jiuziyan and Shuanghe Fms based on $\delta^{18}\text{O}$ (VSMOW) and pollen CA.

Formation	Epoch according to geological map	Epoch according to Goubet et al., 2017	Method	$\delta^{18}\text{O}$ values (‰)	Reference	Lapse rate	$\delta^{18}\text{O}$ at sea level (‰)	Reference	Continental effect?	Paleo-elevation (m)	+	–	Max (m)	Min (m)	No. on Figs. 8& 9	Reference
Baoxiangsi	Eocene/Early Oligocene	Late Eocene	$\delta^{18}\text{O}$, pedogenic carbonates	-9 ± 0.3	Hoke et al., 2014	Paleogene, Hoke et al., 2014	–5.5	Hoke et al., 2014	No	2650	300	300	2950	2350	1	Hoke et al., 2014
Jiuziyan	Miocene	Late Eocene	$\delta^{18}\text{O}$ calcareous mudstones and marls	-8.9 ± 1.2	This study	Paleogene, Hoke et al., 2014	–5.5	Hoke et al., 2014	No	2525	775	725	3300	1800	2a	This study
Jiuziyan	Miocene	Late Eocene	$\delta^{18}\text{O}$ calcareous mudstones and marls	-8.9 ± 1.2	This study	Paleogene, Hoke et al., 2014	–8.2 \pm 1	Licht et al., 2014	No	2525	1475	1425	3900	1150	2b	This study
Jiuziyan	Miocene	Late Eocene	$\delta^{18}\text{O}$ calcareous mudstones and marls	-8.9 ± 1.2	This study	Paleogene, Hoke et al., 2014	–5.5	Hoke et al., 2014	No	500	825	500	1300	0	3a	This study
Jiuziyan	Miocene	Late Eocene	$\delta^{18}\text{O}$ calcareous mudstones and marls	-8.9 ± 1.2	This study	Paleogene, Hoke et al., 2014	–8.2 \pm 1	Licht et al., 2014	No	500	2125	500	2625	0	3b	This study
Jiuziyan	Miocene	Late Eocene	$\delta^{18}\text{O}$ calcareous mudstones and marls	-8.9 ± 1.2	This study	Paleogene, Hoke et al., 2014	–8.2 \pm 1	Licht et al., 2014	Strong	0	300	0	300	0	4	This study
Shuanghe	Middle Miocene	36.2 \pm 0.7 Ma	$\delta^{18}\text{O}$ pedogenic carbonates	-12.1 ± 0.5	Hoke et al., 2014	Modern, Hoke et al., 2014	–5.5	Hoke et al., 2014	No	3300	500	500	3800	2800	5	Hoke et al., 2014
Shuanghe	Middle Miocene	36.2 \pm 0.7 Ma	$\delta^{18}\text{O}$ lacustrine carbonates	-12.44 ± 1.46	Li et al., 2015	Modern, Rowley and Garzzone, 2007	–6.6 \pm 1.4	Li et al., 2015	No	2816	861	1222	3677	1594	6	Li et al., 2015
Shuanghe	Middle Miocene	36.2 \pm 0.7 Ma	$\delta^{18}\text{O}$ lacustrine carbonates re-evaluation of Hoke et al., 2014 and Li, 2015 data	-12.44 ± 1.46	Li et al., 2015	Modern, Rowley and Garzzone, 2007	–6.6 \pm 1.4	Li et al., 2015	Moderate	2601	802	1140	3403	1461	7	Li et al., 2015
Shuanghe	Middle Miocene	36.2 \pm 0.7 Ma	$\delta^{18}\text{O}$ lacustrine carbonates re-evaluation of Hoke et al., 2014 and Li, 2015 data	-9.5 ± 1.2	Hoke et al., 2014; Li et al., 2015	Eocene, Rowley and Garzzone, 2007	–8.2 \pm 1	Licht et al., 2014	No	2800	1000	1000	3800	1800	8	Goubet et al., 2017
Shuanghe	Middle Miocene	36.2 \pm 0.7 Ma	$\delta^{18}\text{O}$ calcareous mudstones and marls	-9.5 ± 1.2	Hoke et al., 2014; Li et al., 2015	Eocene, Rowley and Garzzone, 2007	–8.2 \pm 1	Licht et al., 2014	Strong	1200	1200	1200	2400	0	9	Goubet et al., 2017
Shuanghe	Middle Miocene	36.2 \pm 0.7 Ma	$\delta^{18}\text{O}$ calcareous mudstones and marls	-9.5 ± 1.1	This study	Paleogene, Hoke et al., 2014	–5.5	Hoke et al., 2014	No	2900	675	725	3575	2175	10a	This study
Shuanghe	Middle Miocene	36.2 \pm 0.7 Ma	$\delta^{18}\text{O}$ calcareous mudstones and marls	-9.5 ± 1.1	This study	Paleogene, Hoke et al., 2014	–5.5	Hoke et al., 2014	No	2900	1280	1320	4180	1580	10b	This study
Shuanghe	Middle Miocene	36.2 \pm 0.7 Ma	$\delta^{18}\text{O}$ calcareous mudstones and marls	-9.5 ± 1.1	This study	Paleogene, Hoke et al., 2014	–8.2 \pm 1	Licht et al., 2014	No	900	660	740	1560	160	11a	This study
Shuanghe	Middle Miocene	36.2 \pm 0.7 Ma	$\delta^{18}\text{O}$ calcareous mudstones and marls	-9.5 ± 1.1	This study	Paleogene, Hoke et al., 2014	–8.2 \pm 1	Licht et al., 2014	No	900	1990	900	2890	0	11b	This study

(continued on next page)

Table 4 (continued)

Formation	Epoch according to geological map	Epoch according to Goubet et al., 2017	Method	$\delta^{18}\text{O}$ values (‰)	Reference	Lapse rate	$\delta^{18}\text{O}$ at sea level (‰)	Reference	Continental effect?	Paleo-elevation (m)	+	–	Max (m)	Min (m)	No. on Figs. 8&9	Reference
Shuanghe	Middle Miocene	36.2 ± 0.7 Ma	$\delta^{18}\text{O}$, calcareous mudstones and marls	–9.5 ± 1.1	This study	Paleogene, Hoke et al., 2014	–8.2 ± 1	Licht et al., 2014	Strong	0	700	0	1500	500	12	This study
Shuanghe	Middle Miocene	36.2 ± 0.7 Ma	CA approach on pollen assemblages		This study					1950	650	650	2600	1300	13	This study
Present day										3300	1300	1300	2950	2350	14	

The table shows reconstructed $\delta^{18}\text{O}$ from each sampled formation and previous works. The average isotopic values shown for each formation correspond to the final average isotopic values that we use for paleoelevation calculation.

pollen data (mean value of 19.3 ± 2.5 °C). As lacustrine micrites likely precipitated in lake surface environments, we employ a transfer function used by Hren and Sheldon (2012) to delineate the difference between Mean Annual Lake Surface Temperature (MALST) and MAAT to calculate the most likely temperature at which lacustrine carbonates formed. We consider the MALST transfer function a reasonable choice because our study region resided in the tropics/sub-tropics where seasonal temperature fluctuations were minimal (Hren and Sheldon, 2012). The equation is as follows:

$$\text{MAAT (}^{\circ}\text{C)} = -0.0318 \times T^2 + 2.195 \times T - 12.607 \quad (1)$$

The reconstructed carbonate formation temperature of lacustrine micrites formed in shallow water indicates a MALST of $20.8^{+3.2}_{-2.4}$ °C. We reconstructed the meteoric water isotopic value ($\delta^{18}\text{O}_{\text{mw}}$) from the isotopic composition of carbonates ($\delta^{18}\text{O}_{\text{c}}$) and the carbonate formation temperature inferred above using the temperature-dependent fractionation equation of Kim et al. (2007). The mean $\delta^{18}\text{O}_{\text{mw}}$ (VSMOW) value for the Jiuziyan Fm is -8.9 ± 1.2 ‰, and -9.5 ± 1.1 ‰ for the Shuanghe Fm.

5.3. New paleoelevation estimates and comparisons

Our study area is located on the southeastern margin of the TP. Rayleigh fractionation modeling is appropriate for studying areas of latitude $< 35^{\circ}$ (Rowley and Garzione, 2007); this has been shown to be true on the southeastern margin of the TP based on a comparison of surface water compositions and Rayleigh distillation modeling (Hoke et al., 2014). We calculated paleoelevations from reconstructed $\delta^{18}\text{O}_{\text{mw}}$ values using the variable lapse rate model described by Hoke et al. (2014) that takes into consideration a warmer climate in the Eocene.

Open lake conditions in Eocene lacustrine carbonates (see Section 5.2) allows for the inference that the mean $\delta^{18}\text{O}_{\text{mw}}$ estimates from the sample suite approximate the $\delta^{18}\text{O}$ values of precipitation. Using the relationship linking $\delta^{18}\text{O}_{\text{mw}}$ and altitude proposed by Hoke et al. (2014) for the Eocene, the mean $\delta^{18}\text{O}_{\text{mw}}$ value of -8.9 ± 1.2 ‰ (2 σ) for the lower Jiuziyan Fm micrites corresponds to an elevation range of 2.5 ± 0.7 km asl (2 σ) (Table 4, point 2 and 2a in Fig. 8). The mean $\delta^{18}\text{O}_{\text{mw}}$ value of -9.5 ± 1.1 ‰ (2 σ) for the Shuanghe Fm defines an elevation range of 2.9 ± 0.6 km asl (2 σ) (Table 4, point 10 and 10a in Fig. 8). Note that taking into account the uncertainty defined by the Hoke et al. (2014) Monte Carlo simulation would increase the uncertainties in altitude by ± 700 m (Table 4, point 2b and 10b in Fig. 8). Hoke et al. (2014) assumed that the $\delta^{18}\text{O}$ at the coast was the same in the Eocene as it is today (~ -5.5 ‰), although no constraints on this value existed for the Eocene. However, Licht et al. (2014) have since shown that in the Eocene $\delta^{18}\text{O}$ near the Myanmar coast at this time was much lower (-8.2 ± 1 ‰). Taking this new value as a reference at sea level the Hoke et al. (2014) equation is corrected as follows:

$$Z (\text{m}) = 12.4 \times (\delta^{18}\text{O} - \Delta)^2 - 804 \times (\delta^{18}\text{O} - \Delta) - 3637 \quad (2)$$

where $\Delta = 3.3 \pm 1$ ‰, which is the difference between Licht et al. (2014) Eocene sea level $\delta^{18}\text{O}$ (-8.2 ± 1 ‰) and Hoke simulation result (-4.9 ‰). For the corrected calculation of paleoelevation (Fig. 8), the mean value was obtained by combining the mean $\delta^{18}\text{O}_{\text{mw}}$ in the Jianchuan Basin with the mean coastal $\delta^{18}\text{O}_{\text{mw}}$ (-8.2 ‰), the lowest bound by combining the lowest estimated $\delta^{18}\text{O}_{\text{mw}}$ with the lowest sea level $\delta^{18}\text{O}$ (-9.2 ‰) minus the 700 m uncertainties on Hoke et al. (2014) equation, and the highest bound by combining the highest estimated $\delta^{18}\text{O}_{\text{mw}}$ with the highest sea level $\delta^{18}\text{O}_{\text{mw}}$ (-7.2 ‰) and adding the 700 m uncertainties on Hoke et al. (2014) equation.

Applying this modification results in a lower paleoelevation of $0.5^{+0.8}_{-0.5}$ km asl for the Jiuziyan Fm. (Table 4, point 3 and 3a in Fig. 8), and $0.9^{+0.7}_{-0.7}$ km asl for Shuanghe Fm (point 11 and 11a in Fig. 8). Taking into account the uncertainties on the Hoke et al. (2014) relationship and the $\delta^{18}\text{O}$ value of Licht et al. (2014) yield larger uncertainties (Table 4, point 3b and 11b in Fig. 8). Assuming a significant

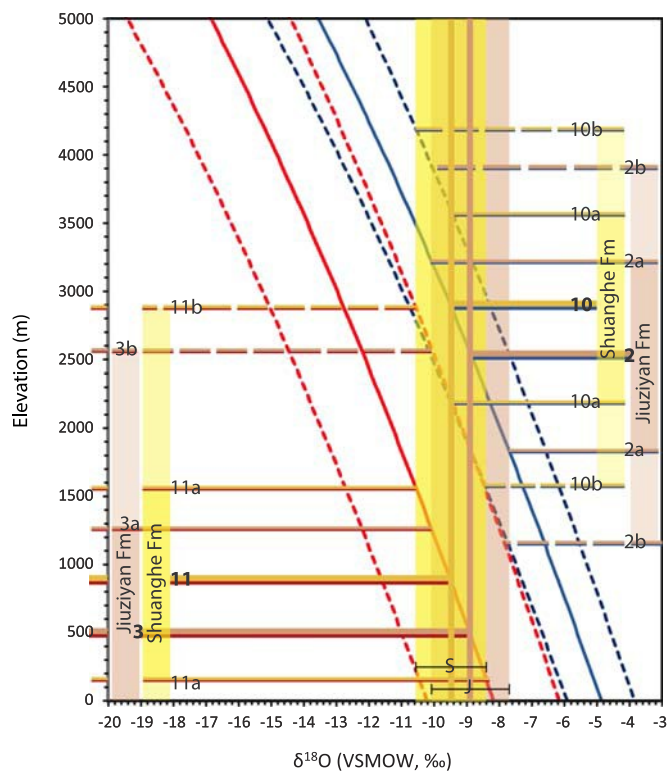


Fig. 8. Relationship between $\delta^{18}\text{O}_{\text{mw}}$ and altitude used to calculate paleoelevation of the Jiuziyan and Shuanghe Fm. The blue continuous line is the average relationship defined by Hoke et al. (2014) with $\delta^{18}\text{O}$ at the seashore equal to -5.5‰ (present day value), while the dashed blue lines correspond to the uncertainty defined by this Monte Carlo simulation. The red continuous line is the Hoke et al. (2014) relationship but assuming a $\delta^{18}\text{O}$ at the coast equal to $-8.2 \pm 1\text{‰}$ (Eocene value in Myanmar, Licht et al., 2014). The dashed red lines reflect the corresponding uncertainties. See text for details. (For interpretation of the references to colour in this figure legend, the reader is referred to the web version of this article.)

continentality effect would further lower the paleoaltitude estimates (point 4 and 12 in Fig. 9). However, this effect is difficult to quantify and may be significantly damped in a warmer world where surface water recycling by evapotranspiration is stronger. Previous studies applied such a correction. Li et al. (2015) considered that the Jianchuan Basin was located 150 km inland, which is an order of magnitude less than Gourbet et al. (2017) who considered a distance of about 1500 km that would convert in an approximately ~ 1000 m elevation correction. Furthermore, the continentality effect at tropical latitude might not be significant as evidenced in the Andes by Insel et al. (2013).

Our study yields two proxies from the Shuanghe Fm (pollen and $\delta^{18}\text{O}_c$) that can be used to constrain paleoelevation during the Late Eocene. Based on the pollen-based CA results, we estimate a paleoelevation of 1.95 ± 0.65 km asl (Table 1, point 13 in Fig. 9). This estimate overlaps with the $\delta^{18}\text{O}_c$ paleoelevation estimates considering that the Eocene lapse rate should be anchored at $\sim -8.2\text{‰}$ (Eocene value in Myanmar) (point 11 in Fig. 9). The intersection between the two proxies (Fig. 9 - red box) corresponds to altitudes of about 1300 to 1600 m (or 2600 m considering all uncertainties), slightly lower than the modern elevation range (3.3 ± 1.3 km, point 14 in Fig. 9). In any case the pollen results are incompatible with estimates that would take into account a significant continentality effect (point 12 in Fig. 9).

We also note that the *Cedripites* taxa composed 4.1% of the principal pollen taxa total. Generally, in areas where living *Cedripites* occur naturally, winters are relatively wet (Su et al., 2013), as the seeds of *Cedripites* germinate immediately when they are mature, and benefit from wet winters in terms of their overall survival rates (Kumar et al.,

2011). Alternatively, the existence of this genus suggests that the study region may not have reached a high elevation. Cross-relating the distribution of vertical vegetation zones to the diverse percentages of particular pollen taxa within the whole, we were able to use the CA method to determine that coniferous/deciduous broad-leaved forests and fern taxa represented the principal types of cover in our study region. Based on this, the maximum overlap of all the NLRs, combined with individual percentages of different pollen taxa, provided a paleoelevation range of 1300–2600 m asl (Fig. 6). We acknowledge that this estimated paleoelevation range is based upon the elevational ranges of modern vegetation equivalents (NLRs) on the southeastern TP. Taking Eocene climatic warming ($\sim 6^\circ\text{C}$ higher than the present day) into consideration, as well as changes in paleogeographic positions due to the Indian-Eurasian continental plate collision (Meyer, 2007), we propose that the raw CA elevational of 1.95 ± 0.65 km asl represents the minimum paleoelevation of this area.

Our paleoelevation results can be compared with previous research results. From the analysis of $\delta^{18}\text{O}$ of lacustrine carbonates of the Shuanghe Fm and taking into account a moderate continentality effect, Li et al. (2015) proposed a paleoaltitude of $2.6 (+0.8/-1.1)$ km (point 7 in Fig. 9). However, they considered that the formation was Early Miocene in age, which lead them to use a modern oxygen stable isotope versus elevation relationship and a Miocene $\delta^{18}\text{O}_c$ reference at low altitude instead of the Late Eocene values, which render their estimate doubtful. Hoke et al. (2014) worked on pedogenetic carbonates of the Baoliangxi Formation near Liming, ~ 50 km north of our sampling locality. They infer a 2.6 ± 0.3 km asl paleoelevation during Late Eocene time (point 1 in Fig. 9). However, they use the MAAT from Sun et al. (2011) of the Shuanghe Fm increased by $+10^\circ\text{C}$, because they thought that the Shuanghe Fm was Miocene in age. Because this formation is in fact Eocene that $+10^\circ\text{C}$ correction appears unjustified and renders their final estimate uncertain. Taking into account the new age constraints for the Shuanghe Fm Gourbet et al. (2017) have reevaluated the data of Hoke et al. (2014) and Sun et al. (2011) to indicate a paleoaltitude of 2.8 ± 1.0 km (point 8 in Fig. 9). They also considered that a continentality effect correction had to be applied to this result and propose a final estimate of 1.2 ± 1.2 km (point 9 in Fig. 9) (Gourbet et al., 2017), although the appropriateness of such a correction in both a tropical climate and a warmer Eocene world is uncertain.

The choice of the value of $\delta^{18}\text{O}_{\text{mw}}$ at low elevation in the Eocene is crucial and makes a large difference in the resulting paleoaltitude estimates. Taking the present-day value would imply that the Jianchuan Basin was at an elevation similar to present day, at the time of sedimentation of the Jiuziyan and Shuanghe Fms during the Late Eocene (~ 36 Ma) (blue arrow, Fig. 8); while taking the values proposed for Myanmar in the Eocene (Licht et al., 2014) would imply that only a fraction of present day elevation was acquired at the time of deposition of the Jiuziyan and Shuanghe Fms, and that additional uplift occurred later on (red arrow, Fig. 8).

5.4. Tectonic and geodynamic implications

A variety of geodynamic models have been proposed for the evolution of southeastern Tibet since the onset of the India-Asia collision. These models have implications on the paleoelevation of the SE Tibetan Plateau and its evolution through time. For example, this region has been viewed as the archetypal model of lower crustal flow from the edges of a continental plateau (e.g., Clark and Royden, 2000). In this model the southeastern TP initially at altitude close to sea level progressively gain altitude above a flow of lower crustal material expelled from below the High TP. Alternatively, other have proposed that crustal thickening has started early after the collision to form an Eocene Tibet including south and southeast Tibet, and that the TP then grew progressively to the north (Tapponnier et al., 2001).

Lower crustal flow has been invoked to explain regional, seemingly synchronous, Late Miocene drainage reorganization and river incision

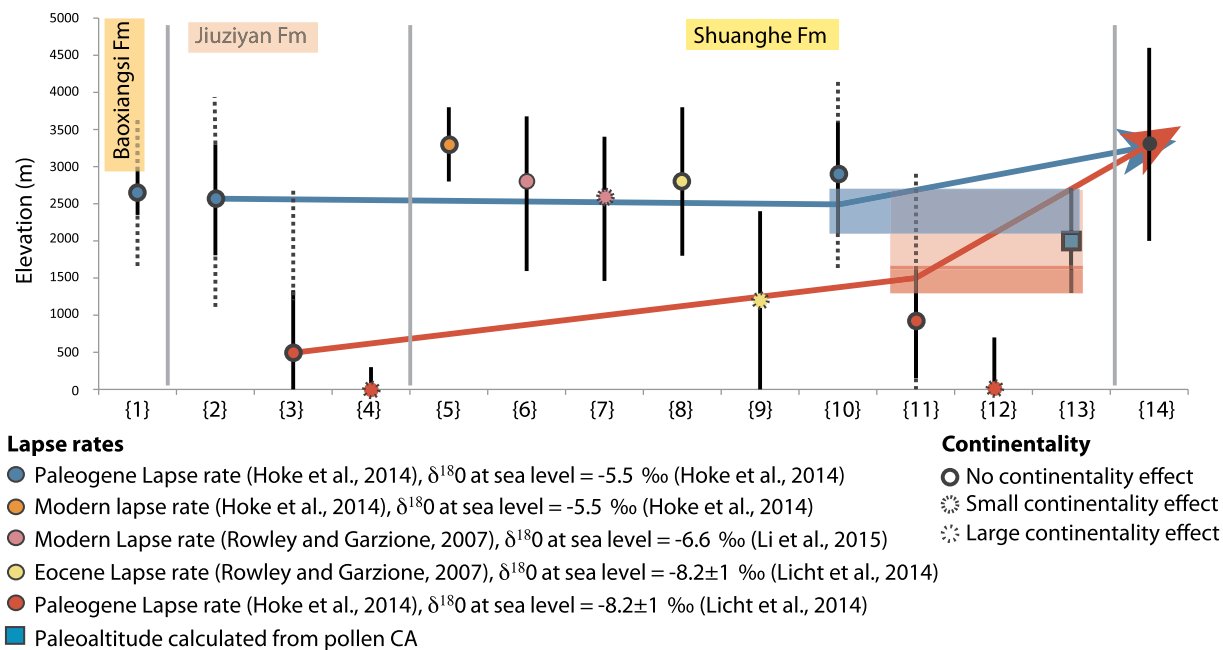


Fig. 9. Altitude estimates for the Jianchuan Basin.

[1] Baoxiangsi Fm from Hoke et al. (2014). [2] Jiuziyan Fm from this study using the Hoke et al. (2014) relationship, [a] uses the average relationship while [b] takes into account the uncertainties on that relationship. [3] Jiuziyan Fm from this study using the modified relationship using the Licht et al. (2014) value of $\delta^{18}\text{O}$ at the coast, [a] uses the average relationship while [b] takes into account the uncertainties on that relationship. [4] corresponds to [3a] but assuming a strong continentality effect. [5] Shuanghe Fm. (Hoke et al., 2014). [6] Shuanghe Fm. (Li et al., 2015). [7] corresponds with [6] but taking into account a moderate continentality effect (Li et al., 2015). [8] Gourbet et al., (2017): Shuanghe Fm. $\delta^{18}\text{O}$ values of Hoke et al. (2014) and Li et al., (2015) but applying the Rowley and Garzzone (2007) relationship with a value of $-8.2 \pm 1\text{‰}$ at sea Level (Licht et al., 2014). [9] Corresponds with [8] but assuming a strong continentality effect (Gourbet et al., 2017). [10] Shuanghe Fm from this study using the Hoke et al. (2014) relationship, [a] uses the average relationship while [b] takes into account the uncertainties on that relationship. [11] Shuanghe Fm from this study using the modified relationship with the Licht et al. (2014) value of $\delta^{18}\text{O}$ at the coast, [a] uses the average relationship while [b] takes into account the uncertainties on that relationship. [12] corresponds to [11a] but assuming a strong continentality effect. [13] altitude range from pollen CA approach (this study). [14] Present day range of altitudes. (For interpretation of the references to colour in this figure legend, the reader is referred to the web version of this article.)

along the northwestern margin of the southeastern TP and the Red River region (e.g., Clark et al., 2004). Clark et al. (2005, 2006) suggested that the magnitude of late Miocene surface uplift can be determined from the timing and magnitude of incision relative to relict low relief paleosurfaces on the Plateau. Thermochronological studies have been used to infer that such flow-induced crustal thickening and surface uplift commenced during the Middle to Late Miocene along the Plateau margins of western Sichuan and southern Yunnan (Kirby et al., 2002; Clark et al., 2005; Godard et al., 2009; Ouimet et al., 2010). However, our study confirms that the Jianchuan Basin was already at relatively high elevation (1300 to 2600 m red box on Fig. 9) at time of deposition in the Upper Eocene, thus prior to the timing inferred for the channel flow and associated uplift. Other studies have suggested that other parts of the southeastern TP have attained high elevation since the Eocene. In the Gonjo Basin, located ~400 km north of the Jianchuan Basin, measurements of $\delta^{18}\text{O}$ in pedogenic carbonates yielded values of $-11.75 \pm 0.35\text{‰}$ corresponding to $\delta^{18}\text{O}_{\text{mw}}$ of $-10 \pm 1.9\text{‰}$ (Tang et al., 2017). From these values these authors infer that the basin was at a minimum average elevation of 2.1–2.5 km during the Early Eocene (43 Myr ago). Note that applying the corrected lapse rate discussed above would yield a lower estimate of ~1200 m. Lacassin et al. (1996) suggested that crustal thickening was taking place in the Yulong anticline, ~50 km NE of the Jianchuan Basin, as early as 36 Myr ago. We thus concur with Tapponnier et al. (2001), Liu-Zeng et al. (2008), Hoke et al. (2014) and Wissink et al. (2016) to suggest that a combination of base-level fall induced by fault-related river captures conspired to create the Late Cenozoic incision signal observed in the tributaries of the Yangtze River, and that high paleoelevation in northwestern Yunnan represented remnants of the Eocene TP that had originally formed in the northeastern Qiangtang Block as a result of

crustal shortening associated with the Indian-Eurasian collision. We consider it unlikely that Middle Miocene crustal flow was responsible for the initial uplift of the southeastern TP.

6. Conclusions

We analyzed marls, calcareous mudstones and ostracod shells from the Eocene Jianchuan Basin on the southeastern TP in order to reconstruct paleoelevation and paleoenvironment. This effort failed in the use clumped isotopes T estimates because diagenetic alteration of the samples during burial has produced high paleotemperatures of up to 90 °C. Additionally, marls and calcareous mudstones showed a large temperature range from 21 °C to 55 °C. The elevated TA_{47} values and micritic nature of the carbonates suggested that diagenesis occurred as solid-state C–O bond reordering. We reconstructed a MAAT of 16.8–21.7 °C for the Late Eocene Jianchuan Basin using a pollen-based CA. This MAAT is ~6 °C warmer than the modern mean air temperature recorded for this area.

Multiproxy-based paleoclimatic reconstructions of the Jianchuan Basin suggested that our study area remained at 2.5 ± 0.7 km asl during the precipitation of the Jiuziyan Fm, while had obtained at 2.9 ± 0.6 km asl by ~36 Ma, accompanied by positive $\delta^{18}\text{O}_{\text{mw}}$ values of $-9.5 \pm 1.1\text{‰}$ (2 σ). However, after modifying by the new value of sea level, these modification results are in a lower paleoelevation of $0.5^{+0.8}_{-0.5}$ km asl for the Jiuziyan Fm. and $0.9^{+0.7}_{-0.7}$ km asl for the Shuanghe Fm. The pollen data appear to indicate that the dominant regional vegetation type was tropical-subtropical, deciduous, coniferous, broadleaf forest. Furthermore, pollen data CA results suggest a paleoelevation of 1.95 ± 0.65 km asl for the same period. Our findings suggest that Miocene lower crustal flow was not the cause of passive surface uplift of

the southeastern TP that rather resulted from crustal thickening during the Eocene.

Acknowledgments

We would like to thank Wenlin Yang, Jiaxuan Wang and Qiong Qin in the field work and Pennilyn Higgins for the assistance with lab work. We also thank Greg Hoke for the help in revising the Rayleigh distillation model. This study was supported by the Geological Survey of China (Nos. 121201004000150013, DD20160345), National Natural Science Foundation of China (#41302279, 41772107, 41672195), and the U.S. NSF (#1211527).

References

- Affek, H.P., Eiler, J.M., 2006. Abundance of mass 47 CO₂ in urban air, car exhaust, and human breath. *Geochim. Cosmochim. Acta* 70 (1), 1–12. <http://dx.doi.org/10.1016/j.gca.2005.08.021>.
- BGMRYP (Bureau of Geology and Mineral Resources of Yunnan Province), 1990. Regional Geology of Yunnan Province, Geological Memoirs, Series 1 (728 p.). Geological Publishing House, Beijing (ISBN 7-116-00567-6).
- BGMRYP (Bureau of Geology and Mineral Resources of Yunnan Province), 1996. Lithostratigraphy of Yunnan Province. China University of Geosciences Press, Wuhan, pp. 211–309 (in Chinese).
- Bonifacie, M., Calmels, D., Eiler, J.M., Horita, J., Chaduteau, C., Vasconcelos, C., Bourrand, J.J., 2017. Calibration of the dolomite clumped isotope thermometer from 25 to 350 °C, and implications for a universal calibration for all (Ca, Mg, Fe) CO₃ carbonates. *Geochim. Cosmochim. Acta* 200, 255–279.
- Cao, S., Liu, J., Leiss, B., Neubauer, F., Genser, J., Zhao, C., 2011. Oligo-Miocene shearing along the Ailao Shan–Red River shear zone: constraints from structural analysis and zircon U/Pb geochronology of magmatic rocks in the Diancang Shan massif, SE Tibet, China. *Gondwana Res.* 19 (4), 975–993.
- Chanton, J., Chaser, L., Glasser, P., Sieger, D., 2005. Carbon and hydrogen isotopic effects in microbial methane from terrestrial environments. Chapter 6. In: Flanagan, L.B., Ehleringer, J.R. (Eds.), *Stable Isotopes and Biosphere - Atmosphere Interactions: Processes and Biological Controls*.
- Chung, S.L., Lo, C.H., Lee, T.Y., Zhang, Y.Q., Xie, Y.W., Li, X.H., et al., 1998. Diachronous uplift of the Tibetan Plateau starting 40 myr ago. *Nature* 394 (6695), 769–773.
- Chung, S.L., Chu, M.F., Zhang, Y., Xie, Y., Lo, C.H., Lee, T.Y., et al., 2005. Tibetan tectonic evolution inferred from spatial and temporal variations in post-collisional magmatism. *Earth-Sci. Rev.* 68 (3), 173–196.
- Clark, M.K., Royden, L.H., 2000. Topographic ooze: building the eastern margin of Tibet by lower crustal flow. *Geology* 28, 703–706.
- Clark, M.K., Schoenbohm, L.M., Royden, L.H., Whipple, K.X., Burchfiel, B.C., Zhang, X., Tang, W., Wang, E., Chen, L., 2004. Surface uplift, tectonics, and erosion of eastern Tibet from large-scale drainage patterns. *Tectonics* 23, TC1006. <http://dx.doi.org/10.1029/2002TC001402>.
- Clark, M.K., House, M.A., Royden, L.H., Whipple, K.X., Burchfiel, B.C., Zhang, X., Tang, W., 2005. Late Cenozoic uplift of southern Tibet. *Geology* 33, 525–528.
- Clark, M.K., Royden, L.H., Whipple, K.X., Burchfiel, B.C., Zhang, X., Tang, W., 2006. Use of a regional, relict landscape to measure vertical deformation of the eastern Tibetan Plateau. *J. Geophys. Res.* 111, F03002.
- Decelles, P.G., Robinson, D.M., Zandt, G., 2002. Implications of shortening in the Himalayan fold-thrust belt for uplift of the Tibetan Plateau. *Tectonics* 21 (6), 12–12–25.
- Dennis, K.J., Affek, H.P., Passey, B.H., Schrag, D.P., Eiler, J.M., 2011. Defining an absolute reference frame for “clumped” isotope studies of CO₂. *Geochim. Cosmochim. Acta* 75 (22), 7117–7131. <http://dx.doi.org/10.1016/j.gca.2011.09.025>.
- Eiler, J.M., 2007. “Clumped-isotope” geochemistry—the study of naturally-occurring, multiply-substituted isotopologues. *Earth Planet. Sci. Lett.* 262 (3), 309–327. <http://dx.doi.org/10.1016/j.epsl.2007.08.020>.
- Eiler, J.M., 2011. Paleoclimate reconstruction using carbonate clumped isotope thermometry. *Quat. Sci. Rev.* 30 (25), 3575–3588. <http://dx.doi.org/10.1016/j.quascirev.2011.09.001>.
- Eiler, J.M., Schauble, E., 2004. ¹⁸O¹³C¹⁶O in Earth's atmosphere. *Geochim. Cosmochim. Acta* 68 (23), 4767–4777. <http://dx.doi.org/10.1016/j.gca.2004.05.035>.
- Enkelmann, E., Ratschbacher, L., Jonckheere, R., Nestler, R., Fleischer, M., Gloaguen, R., Hacker, B.R., Zhang, Y., Ma, Y., 2006. Cenozoic exhumation and deformation of northeastern Tibet and the Qinling: is Tibetan lower crustal flow diverging around the Sichuan Basin? *Geol. Soc. Am. Bull.* 118, 651–671.
- Faegri, K., Iversen, J., 1989. *Textbook of Pollen Analysis*, 4th ed. Wiley Press, New York, pp. 1–328.
- Garzione, C.N., Dettman, D.L., Horton, B.K., 2004. Carbonate oxygen isotope paleoaltimetry: evaluating the effect of diagenesis on paleoelevation estimates for the Tibetan Plateau. *Palaeogeogr. Palaeoclimatol. Palaeoecol.* 212 (1), 119–140. <http://dx.doi.org/10.1016/j.palaeo.2004.05.020>.
- Ghosh, P., Adkins, J., Affek, H., Balta, B., Guo, W.F., Schauble, E.A., Schrag, D., Eiler, J.M., 2006. ¹³C–¹⁸O bonds in carbonate minerals: a new kind of paleothermometer. *Geochim. Cosmochim. Acta* 70 (6), 1439–1456. <http://dx.doi.org/10.1016/j.gca.2005.11.014>.
- Gilley, L.D., Harrison, T.M., Leloup, P.H., Ryerson, F.J., Lovera, O.M., Wang, J.H., 2003. Direct dating of left-lateral deformation along the Red River shear zone, China and Vietnam. *J. Geophys. Res. Solid Earth* 108 (B2).
- Godard, V., Pik, R., Lavé, J., Cattin, R., Tibari, B., de Sigoyer, J., Pubellier, M., 2009. Late Cenozoic evolution of the central Longmen Shan, eastern Tibet: insight from (U–Th)/He thermochronometry. *Tectonics* 28 (5), TC5009. <http://dx.doi.org/10.1029/2008TC002407>.
- Gourbet, L., Leloup, P.H., Paquette, J.L., Sorrel, P., Maheo, G., Wang, G.C., et al., 2017. Reappraisal of the jianchuan cenozoic basin stratigraphy and its implications on the tibetan plateau evolution. *Tectonophysics* 700–701, 162–179.
- Hoke, G.D., Zeng, J.L., Hren, M.T., Wissink, G.K., Garzione, C.N., 2014. Stable isotopes reveal high southeast Tibetan Plateau margin since the Paleogene. *Earth Planet. Sci. Lett.* 394, 270–278.
- Hren, M.T., Sheldon, N.D., 2012. Temporal variations in lake water temperature: paleoenvironmental implications of lake carbonate ^δ18O and temperature records. *Earth Planet. Sci. Lett.* 337–338, 77–84. <http://dx.doi.org/10.1016/j.epsl.2012.05.019>.
- Huber, M., Goldner, A., 2012. Eocene monsoons. *J. Asian Earth Sci.* 44 (1), 3–23. <http://dx.doi.org/10.1016/j.jseas.2011.09.014>.
- Huntington, K.W., Saylor, J., Quade, J., Hudson, A.M., 2015. High late Miocene–Pliocene elevation of the Zhada Basin, southwestern Tibetan Plateau, from carbonate clumped isotope thermometry. *Geol. Soc. Am. Bull.* 127 (1–2), 181–199. <http://dx.doi.org/10.1130/B31000.1>.
- Insel, N., Poulsen, C.J., Sturm, C., Ehlers, T.A., 2013. Climate controls on Andean precipitation ^δ18O interannual variability. *J. Geophys. Res.-Atmos.* 118 (17), 9721–9742.
- Jahren, A.H., Lepage, B.A., Werts, S.P., 2004. Methanogenesis in Eocene Arctic soils inferred from ^δ13C of tree fossil carbonates. *Palaeogeogr. Palaeoclimatol. Palaeoecol.* 214, 347–358.
- Ji, L., Qiao, Z., Zhang, H., Meng, F., 2007. Micropalaeontology of Eocene lower Ganchaigou Formation in the Kuntuyi depression of the northern margin of the Qaidam Basin. *Acta Microbiol. Sin.* 24 (1), 82–88.
- Jiang, G., Yuan, A., Zhang, K., 2014. The ostracod fauna and its geological significance from the Late Eocene Kangtuo Formation, the Gaize Basin, southern Tibet Plateau, China. *Acta Microbiol. Sin.* 31 (4), 405–419.
- Kim, S.T., O'Neil, J.R., Hillaire-Marcel, C., Mucci, A., 2007. Oxygen isotope fractionation between synthetic aragonite and water: influence of temperature and Mg²⁺ concentration. *Geochim. Cosmochim. Acta* 71 (19), 4704–4715. <http://dx.doi.org/10.1016/j.gca.2007.04.019>.
- Kirby, E., Reiners, P.W., Krol, M.A., Whipple, K.X., Hodges, K.V., Farley, K.A., Tang, W., Chen, Z., 2002. Late Cenozoic evolution of the eastern margin of the Tibetan Plateau: inferences from 40Ar/39Ar and (U–Th)/He thermochronology. *Tectonics* 21 (1). <http://dx.doi.org/10.1029/2000TC001246>.
- Kumar, R., Singh, C., Malik, S., Ali, A., Nayital, R.K., 2011. Effect of storage conditions on germinability of Himalayan Cedar (*Cedrus deodara* Roxb., G. Don) seeds. *Indian Forester* 137, 1099–1102.
- Lacassin, R., Schärer, U., Leloup, P.H., Arnaud, N., Tapponnier, P., Liu, X., Zhang, L., 1996. Tertiary deformation and metamorphism SE of Tibet: the folded Tiger-leap décollement of NW Yunnan, China. *Tectonics* 15 (3), 605–622.
- Leloup, P.H., Tapponnier, P., Lacassin, R., Searle, M.P., 2007. Discussion on the role of the Red River shear zone, Yunnan and Vietnam, in the continental extrusion of SE Asia. *Journal*, vol. 163, 2006, 1025–1036. *J. Geol. Soc.* 164 (6), 1253–1260.
- Li, D.R., Huang, X.G., Wang, A.D., Yu, S.E., 1987. The discovery and its significance of marine limestone in early Tertiary, Northwest Yunnan. *Chin. Sci. Bull.* 292–296.
- Li, S.Y., Currie, S., Brian, Rowley, B. David, Miquela, Ingalls, 2015. Cenozoic paleoaltimetry of the SE margin of the Tibetan Plateau: constraints on the tectonic evolution of the region. *Earth Planet. Sci. Lett.* 432, 415–424.
- Liang, H.Y., Campbell, I.H., Allen, C.M., Sun, W.D., Yu, H.X., Xie, Y.W., Zhang, Y.Q., 2007. The age of the potassic alkaline igneous rocks along the Ailao Shan–Red River shear zone: implications for the onset age of left-lateral shearing. *J. Geol.* 115 (2), 231–242.
- Licht, A., Van Cappelle, M., Abels, H.A., Ladant, J.B., Trabuco-Alexandre, J., France-Lanord, C., Terry Jr., D., 2014. Asian monsoons in a late Eocene greenhouse world. *Nature* 513 (7519), 501.
- Liu-Zeng, J., Tapponnier, P., Gaudemer, Y., Ding, L., 2008. Quantifying landscape differences across the Tibetan plateau: implications for topographic relief evolution. *J. Geophys. Res. Earth Surf* (2003–2012).
- Lu, Y.J., Kerrich, R., Cawood, P.A., McCuaig, T.C., Hart, C.J.R., Li, Z.X., Bagas, L., 2012. Zircon shrimp U–Pb geochronology of potassic felsic intrusions in western Yunnan, SW China: constraints on the relationship of magmatism to the Jinsha suture. *Gondwana Res.* 22 (2), 737–747.
- Ma, H.J., 2013. Cenozoic Stratigraphy and Paleoenvironmental Changes in the Hengduan Mountains Region, Southwest China. Kunming University of Science and Technology.
- Meyer, H.W., 2007. A review of paleotemperature-lapse rate methods for estimating paleoelevation from fossil floras. *Rev. Mineral. Geochem.* 66, 155–171.
- Miao, Y., Wu, F., Chang, H., Fang, X., Deng, T., Sun, J., Jin, C., 2016. A Late-Eocene palynological record from the Hoh Xil Basin, northern Tibetan Plateau, and its implications for stratigraphic age, paleoclimate and paleoelevation. *Gondwana Res.* 31, 241–252.
- Molnar, P., Tapponnier, P., 1975. Cenozoic tectonics of Asia: effects of a continental collision. *Science* 189 (4201), 419–426.
- Mosbrugger, V., Utescher, T., 1997. The coexistence approach—a method for quantitative reconstructions of Tertiary terrestrial paleoclimate data using plant fossils. *Palaeogeogr. Palaeoclimatol. Palaeoecol.* 134, 61–86.
- Ouimet, W., Whipple, K., Royden, L., Reiners, P., Hodges, K., Pringle, M., 2010. Regional incision of the eastern margin of the Tibetan Plateau. *Lithosphere* 2 (1), 50–63.
- Palin, R.M., Searle, M.P., Waters, D.J., Parrish, R.R., Roberts, N.M.W., Horstwood, M.S.A., et al., 2013. A geochronological and petrological study of anatectic paragneiss and associated granite dykes from the day Nui con voi metamorphic core complex, North

- Vietnam: constraints on the timing of metamorphism within the red river shear zone. *J. Metamorph. Geol.* 31 (4), 359–387.
- Passey, B.H., Levin, N.E., Cerling, T.E., Brown, F.H., Eiler, J.M., 2010. High-temperature environments of human evolution in East Africa based on bond ordering in paleosol carbonates. *Proc. Natl. Acad. Sci.* 107 (25), 11245–11249. <http://dx.doi.org/10.1073/pnas.1001824107>.
- Qin, Q., 2017. Sedimentary Character and Paleoenvironmental Research on the Volcanic Event of the Jianchuan Formation in the Jianchuan Basin, Western Yunnan Province. China University of Geosciences.
- Roe, G.H., Ding, Q., Battisti, D.S., Molnar, P., Clark, M.K., Garzione, C.N., 2016. A modeling study of the response of Asian summertime climate to the largest geological forcings of the past 50 Ma. *J. Geophys. Res.-Atmos.* 121 (10), 5453–5470. <http://dx.doi.org/10.1002/2015JD024370>.
- Rowley, D.B., Garzione, C.N., 2007. Stable isotope-based paleoaltimetry. *Annu. Rev. Earth Planet. Sci.* 35, 463–508. <http://dx.doi.org/10.1146/annurev.earth.35.031306.140155>.
- Shen, X., Tian, Y., Li, D., Qin, S., Vermeesch, P., Schwanethal, J., 2016. Oligocene-Early Miocene river incision near the first bend of the Yangze River: insights from apatite (U-Th-Sm)/He thermochronology. *Tectonophysics* 687, 223–231.
- Song, Z.C., Zheng, Y.H., Li, M.N., 1999. Fossil Spores and Pollen of China (I): Late of Cretaceous–Tertiary Spores and Pollen. Science Press, Beijing, pp. 749–757 (in Chinese).
- Song, X.Y., Spicer, R.A., Yang, J., Yao, Y.F., Li, C.S., 2010. Pollen evidence for an Eocene to Miocene elevation of central southern Tibet predating the rise of the High Himalaya. *Palaeogeogr. Palaeoclimatol. Palaeoecol.* 297 (1), 159–168.
- Song, B., Zhang, K., Lu, J., Wang, C., Xu, Y., 2013. The middle Eocene to early Miocene integrated sedimentary record in the Qaidam Basin and its implications for paleo-climate and early Tibetan Plateau uplift. *Can. J. Earth Sci.* 50 (2), 183–196.
- Sorrel, P., Eymard, I., Leloup, P.-H., Maheo, G., Olivier, N., Sterb, M., Gourbet, L., Wang, G., Jing, W., Lu, H., Li, H., Yadong, X., Zhang, K., Cao, K., Chevalier, M.L., Replumaz, A., 2017. Wet tropical climate in SE Tibet during the Late Eocene. *Sci. Rep.* 7, 7809 (DOI:10.1038/s41598-017-07766-9).
- Su, T., Liu, Y.S., Yang, J., Jacques, Frédéric M.B., Huang, Y.J., Xing, Y.W., Zhou, Z.K., 2013. The intensification of the East Asian winter monsoon contributed to the disappearance of *Cedrus* (Pinaceae) in southwestern China. *Quat. Res.* 80, 316–325.
- Sun, B.N., Wu, J.Y., Liu, Y.S.C., Ding, S.T., Li, X.C., Xie, S.P., Yan, D.F., Lin, Z.C., 2011. Reconstructing Neogene vegetation and climates to infer tectonic uplift in western Yunnan, China. *Palaeogeogr. Palaeoclimatol. Palaeoecol.* 304 (3), 328–336.
- Sun, J.M., Xu, Q.H., Liu, W.M., Zhang, Z.Q., Xue, L., Zhao, P., 2014. Palynological evidence for the Latest Oligocene–Early Miocene paleoelevation estimate in the Lunpola Basin, central Tibet. *Palaeogeogr. Palaeoclimatol. Palaeoecol.* 399, 21–30.
- Talbot, M.R., 1990. A review of the paleohydrological interpretation of carbon and oxygen isotopic ratios in primary lacustrine carbonates. *Chem. Geol.* 80, 261–279.
- Talbot, M.R., Kelts, K., 1990. Paleolimnological Signatures From Carbon and Oxygen Isotopic Ratios in Carbonates, from Organic Carbon-rich Lacustrine Sediments (Chapter 6). pp. 99–112.
- Tang, M., Jing, L.Z., Hoke, G.D., Xu, Q., Wang, W., Li, Z., et al., 2017. Paleoelevation reconstruction of the Paleocene-Eocene Gonjo Basin, se-central Tibet. *Tectonophysics* 712–713, 170–181.
- Tapponnier, P., Zhiqin, X., Roger, F., Meyer, B., Arnaud, N., Wittlinger, G., Jingsui, Y., 2001. Oblique stepwise rise and growth of the Tibet Plateau. *Science* 294 (5547), 1671–1677.
- Tong, C., Chen, C., 1992. Early Tertiary Ostracodes from southwest region of Shandong. *Shandong Geol.* 8, 1–18.
- Utescher, T., Mosbrugger, V., 1990–2006. The Palaeoflora database. <http://www.palaeoflora.de>.
- Utescher, T., Ivanov, D., Harzhauser, M., Bozukov, V., Ashraf, A.R., Rolf, C., Urbat, M., Mosbrugger, V., 2009. Cyclic climate and vegetation change in the Late Miocene of Western Bulgaria. *Palaeogeogr. Palaeoclimatol. Palaeoecol.* 272 (1), 99–114.
- Waldron, S., Hall, A.J., Fallick, A.E., 1999. Enigmatic stable isotope dynamics of deep peat methane. *Glob. Biogeochem. Cycles* 13 (1), 93–100.
- Wang, J.H., Yin, A., Harrison, T.M., Grove, M., Zhang, Y.Q., Xie, G.H., 2001. A tectonic model for Cenozoic igneous activities in the eastern Indo-Asian collision zone. *Earth Planet. Sci. Lett.* 188 (1), 123–133.
- Wang, E., Kirby, E., Furlong, K.P., Soest, van M., Xu, G., Shi, X., Knap, P.J.J., Hodges, K.V., 2012. Two-phase growth of high topography in eastern Tibet during the Cenozoic. *Nat. Geosci.* 5 (9), 640–645. <http://dx.doi.org/10.1038/ngeo1538>.
- Wei, H.H., Wang, E., Wu, G.L., Meng, K., 2016. No sedimentary records indicating southerly flow of the paleo-Upper Yangtze River from the First Bend in southeastern Tibet. *Gondwana Res.* 32, 93–104.
- Wilson, C.J., Fowler, A.P., 2011. Denudational response to surface uplift in east Tibet: evidence from apatite fission-track thermochronology. *Geol. Soc. Am. Bull.* 123 (9–10), 1966–1987.
- Wissink, G., Hoke, G.D., Garzione, C.N., Liu-Zeng, Jing, 2016. Temporal and spatial patterns of sediment routing across the southeast margin of the Tibetan Plateau: insights from detrital zircon. *Tectonics* 35. <http://dx.doi.org/10.1002/2016TC004252>.
- Wolfe, J.A., 1993. A method for obtaining climate parameters from leaf assemblages: U.S. Geol. Den. Surv. Bull. 2040 (1993), 1–71.
- Wu, C.Y., 1983. *Flora Xizangica*. vol. 1 Science Press, Beijing.
- Wu, C.Y., 1985. *Flora Xizangica*. vol. 2 Science Press, Beijing.
- Wu, C.Y., 1986a. *Flora Xizangica*. vol. 3 Science Press, Beijing.
- Wu, C.Y., 1986b. *Flora Xizangica*. vol. 4 Science Press, Beijing.
- Wu, C.Y., 1987. *Flora Xizangica*. vol. 5 Science Press, Beijing.
- Xiang, H.F., Zhang, B.L., Zhang, W.X., Guo, S.M., Wan, J.L., 2009. Geological analysis and FT dating of crustal deformation in the Jianchuan Basin since the Tertiary. *Acta Geol. Sin.* 83 (2), 230–238.
- Xiao, C., Ye, M., He, T., 2013. Eocene-Miocene event stratigraphy of southwestern Qaidam Basin. *J. Stratigr.* 2, 242–249.
- Xu, J., Jiang, F., Gao, P., Liu, H., Wang, Y., 2004. Ostracoda Assemblages from the third and fourth members of the Palaeogene Shahejie Formation and their boundary in the Dongpu depression. *J. Stratigr.* 28, 87–91.
- Yang, P., Sun, Z.C., Li, D.M., Jing, M.C., Xu, F.T., Liu, H.M., 2000. Ostracoda extinction and explosion events of the Mesozoic–Cenozoic in Qaidam Basin, Northwest China. *J. Palaeogeogr.* 2 (3), 69–74.
- Zhang, L.S., Schärer, U., 1999. Age and origin of magmatism along the Cenozoic Red River shear belt, China. *Contrib. Mineral. Petrol.* 134 (1), 67–85.
- Zhang, K.X., Wang, G.C., Cao, K., Liu, C., Xiang, S.Y., Hong, H.L., et al., 2008. Cenozoic sedimentary records and geochronological constraints of differential uplift of the Qinghai-Tibet Plateau. *Sci. China Ser. D Earth Sci.* 51 (11), 1658–1672.
- Zhang, K.X., Wang, G.C., Xu, Y.D., Luo, M.S., Ji, J.L., Xiao, G.Q., Wang, A., Song, B.W., Liang, Y.P., Jiang, S.S., Cao, K., Chen, R.M., Yang, Y.F., 2013. Sedimentary evolution of the Qinghai-Tibet Plateau in Cenozoic and its response to the uplift of the Plateau. *Acta Geol. Sin. (English edition)* 87 (2), 555–575.
- Zhao, G.G., 1965. Preliminary observation of the Cenozoic strata and its structure in Dali and Lijiang region, Northwest Yunnan. *Geogr. Rev.* 05, 345–358.
- Zhu, Z., Wu, L., Xi, P., 1985. A Research on Tertiary Palynology From the Qaidam Basin, Qinghai Province. Petroleum Industry Press., Beijing, pp. 1–297.